

# Asgard archaea illuminate the origin of eukaryotic cellular complexity

Katarzyna Zaremba-Niedzwiedzka<sup>1\*</sup>, Eva F. Caceres<sup>1\*</sup>, Jimmy H. Saw<sup>1\*</sup>, Disa Bäckström<sup>1</sup>, Lina Juzokaite<sup>1</sup>, Emmelien Vancaester<sup>1†</sup>, Kiley W. Seitz<sup>2</sup>, Karthik Anantharaman<sup>3</sup>, Piotr Starnawski<sup>4</sup>, Kasper U. Kjeldsen<sup>4</sup>, Matthew B. Stott<sup>5</sup>, Takuro Nunoura<sup>6</sup>, Jillian F. Banfield<sup>3</sup>, Andreas Schramm<sup>4</sup>, Brett J. Baker<sup>2</sup>, Anja Spang<sup>1</sup> & Thijs J. G. Ettema<sup>1</sup>

The origin and cellular complexity of eukaryotes represent a major enigma in biology. Current data support scenarios in which an archaeal host cell and an alphaproteobacterial (mitochondrial) endosymbiont merged together, resulting in the first eukaryotic cell. The host cell is related to Lokiarchaeota, an archaeal phylum with many eukaryotic features. The emergence of the structural complexity that characterizes eukaryotic cells remains unclear. Here we describe the ‘Asgard’ superphylum, a group of uncultivated archaea that, as well as Lokiarchaeota, includes Thor-, Odin- and Heimdallarchaeota. Asgard archaea affiliate with eukaryotes in phylogenomic analyses, and their genomes are enriched for proteins formerly considered specific to eukaryotes. Notably, thorarchaeal genomes encode several homologues of eukaryotic membrane-trafficking machinery components, including Sec23/24 and TRAPP domains. Furthermore, we identify thorarchaeal proteins with similar features to eukaryotic coat proteins involved in vesicle biogenesis. Our results expand the known repertoire of ‘eukaryote-specific’ proteins in Archaea, indicating that the archaeal host cell already contained many key components that govern eukaryotic cellular complexity.

The origin of the eukaryotic cell is regarded as one of the major evolutionary innovations in the history of life on our planet. Yet, the emergence of the complex and compartmentalized nature of eukaryotic cells represents a major conundrum in modern biology<sup>1–3</sup>. Most recent insights support symbiogenic scenarios of eukaryotic evolution<sup>3,4</sup>—that the emergence of the first eukaryotic cell was triggered by a merger between an archaeal host cell<sup>5–9</sup> and an alphaproteobacterial (mitochondrial) endosymbiont<sup>10</sup>. Whereas the alphaproteobacterial provenance of mitochondria is overwhelming, the identity and nature of the archaeal host cell have remained elusive until recently. The identification and genomic characterization of Lokiarchaeota, a clade of archaea found in deep marine sediments, has provided several crucial insights into the archaeal origin of eukaryotes<sup>11</sup>. First, phylogenomic analyses of carefully selected genomic data sets placed Lokiarchaeota as the most closely related group to eukaryotes, providing further compelling evidence for the two-domain tree of life<sup>12</sup>, in which eukaryotes branch from within the archaeal domain. Furthermore, a careful analysis of genome content of the composite Lokiarchaeum genome revealed that it encodes a multitude of genes that were previously regarded specific to eukaryotes<sup>11</sup>. These so-called eukaryotic signature proteins<sup>13</sup> included several cytoskeletal components (actin homologues and gelsolin-domain proteins), ESCRT complex proteins (including ESCRT-I, -II and -III components), and a wide variety of small GTPases<sup>11</sup>, including Gtr/Rag family GTPase orthologues<sup>14,15</sup>—proteins that in eukaryotes are involved in various regulatory processes including cytoskeleton remodelling, signal transduction, nucleocytoplasmic transport and vesicular trafficking. The discovery of Lokiarchaeota has reignited debates about the nature of the archaeal host cell from which eukaryotes emerged. For example, on the basis of analyses of the available lokiarchaeal genome data, inferences have been made about its level of cellular complexity<sup>14,16–19</sup> its membrane composition<sup>20</sup> and its

metabolism<sup>21,22</sup>, leading to renewed efforts to explain the origin and early evolution of eukaryotes. Though insightful, these deductions are preliminary as they are based, so far, on a single genomic data set. Here we describe the metagenomic discovery of the Asgard superphylum, which, as well as Lokiarchaeota, includes several new uncultivated archaeal lineages that reside in a wide variety of environments. We show that these lineages comprise novel phylum-level groups that represent the closest archaeal relatives of eukaryotes. Detailed analyses of their reconstructed genomes provide new insights into the identity and genetic nature of the archaeal ancestor of eukaryotes and the primal stages of eukaryogenesis.

## Metagenomic discovery of Asgard archaea

To gain insight into the archaea-to-eukaryote transition, we aimed to identify and characterize novel archaeal lineages related to the recently described Lokiarchaeota<sup>11</sup>, an archaeal clade that was previously shown to be more closely related to eukaryotes than any other prokaryotic lineage. We sampled aquatic sediments from seven geographically separated sites which differed markedly with respect to their biological and chemical parameters: Loki’s Castle, Yellowstone National Park, Aarhus Bay, an aquifer near Colorado River, Radiata Pool, Taketomi Island Vent and the White Oak River estuary (Extended Data Fig. 1a, Supplementary Table 1). Total DNA was extracted from all samples and sequenced, resulting in a total of 644.88 gigabase pairs (Gbp) of paired end reads. Sequence assembly generated a total of 3.28 Gbp of contiguous sequences (contigs)  $\geq 5$  kb (Supplementary Table 2). To assess the presence of potential Lokiarchaeota-related lineages, contigs containing at least six genes of a conserved 15-ribosomal protein (RP15) gene cluster were extracted and subjected to phylogenomic analysis. This analysis revealed the presence of numerous archaeal contigs that were relatively closely related to the previously described Lokiarchaeota<sup>11</sup>.

<sup>1</sup>Department of Cell and Molecular Biology, Science for Life Laboratory, Uppsala University, SE-75123 Uppsala, Sweden. <sup>2</sup>Department of Marine Science, University of Texas-Austin, Marine Science Institute, Port Aransas, Texas 78373, USA. <sup>3</sup>Department of Earth and Planetary Sciences, and Department of Environmental Science, Policy, and Management, University of California, Berkeley, California, USA. <sup>4</sup>Section for Microbiology and Center for Geomicrobiology, Department of Bioscience, Aarhus University, DK-8000 Aarhus, Denmark. <sup>5</sup>GNS Science, Extremophile Research Group, Private Bag 2000, Taupō 3352, New Zealand. <sup>6</sup>Research and Development Center for Marine Biosciences, Japan Agency for Marine-Earth Science and Technology, Yokosuka 237-0061, Japan.

†Present address: Department of Plant Systems Biology, VIB and Department of Plant Biotechnology and Bioinformatics, Ghent University, Technologiepark 927, B-9052 Ghent, Belgium.

\*These authors contributed equally to this work.

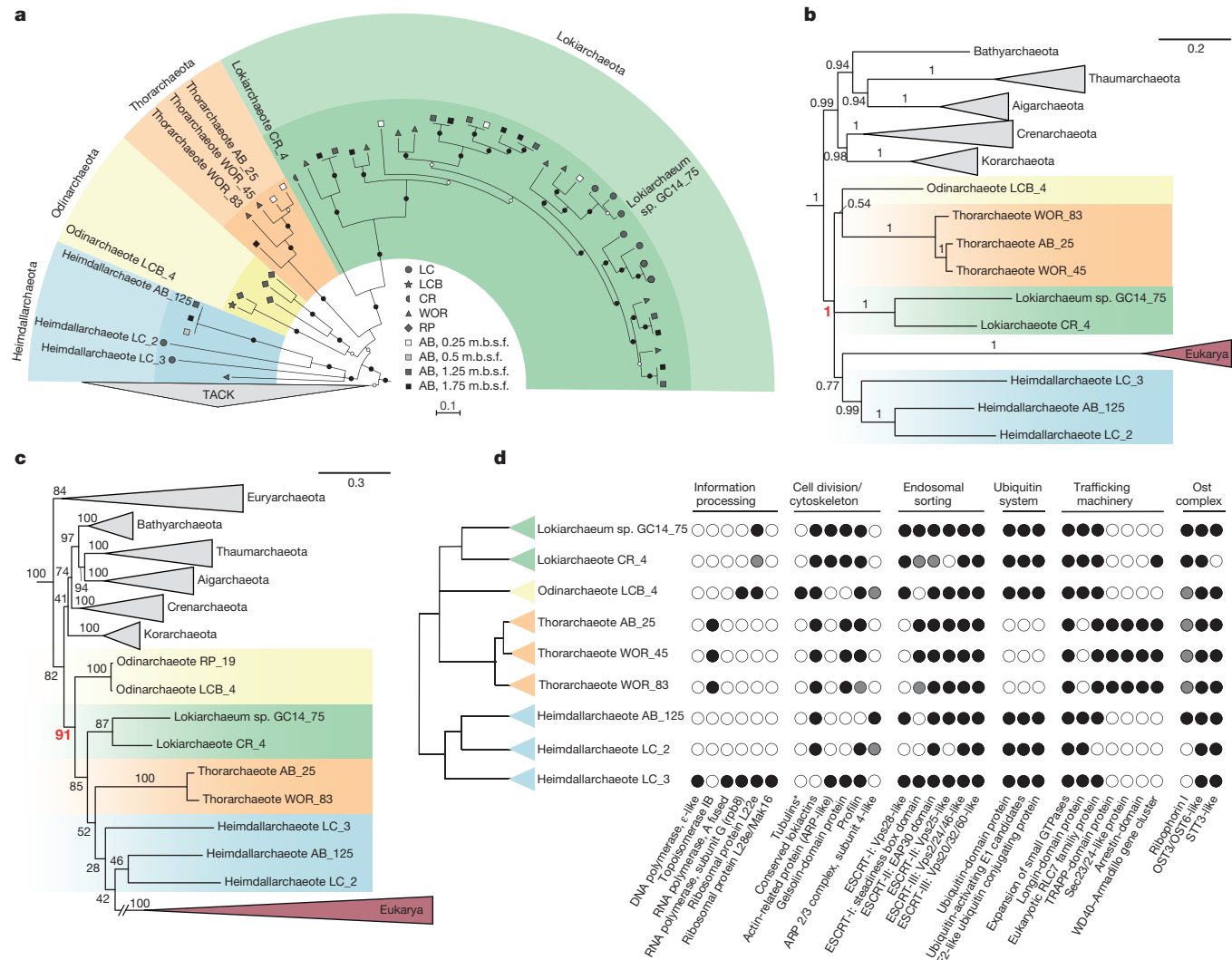


**Figure 1 | Identification and phylogenomics of Asgard archaea.** **a**, Maximum-likelihood tree, inferred with RAxML and PROTCATLG model, based on metagenomic contigs containing conserved ribosomal proteins (see Methods) revealing the Asgard superphylum. Slow, non-parametric maximum-likelihood bootstrap support values above 50 and 90 are indicated with empty and filled circles, respectively. Abbreviations of the sites mentioned are as follows: LC, Loki's Castle; CR, Colorado River aquifer (USA); LCB, Lower Culex Basin (Yellowstone National Park, USA); WOR, White Oak River (USA); AB, Aarhus Bay (Denmark); RP, Radiata Pool (New Zealand); m.b.s.f., metres below sea floor. **b**, Bayesian inference of 55 concatenated archaeo-eukaryotic ribosomal proteins inferred with PhyloBayes and CAT-GTR model (**b**) and maximum-likelihood analysis of concatenated small and large subunit rRNA gene

and Thorarchaeota<sup>23</sup> phyla, but we also identified several sequences that were only distantly related but still part of the same archaeal clade (Fig. 1a). We decided to name this archaeal clade Asgard, after the realm of the gods in Norse mythology. Apart from Lokiarchaeota- and Thorarchaeota-related lineages, we could define two additional candidate phyla in the Asgard clade, which we hereafter refer to as Odinarchaeota and Heimdallarchaeota (Supplementary Table 3, Supplementary Discussion 1). Whereas contigs from Odinarchaeota were exclusively identified in hot spring metagenomes (Yellowstone National Park and Radiata Pool), contigs from Heimdallarchaeota were detected in marine sediments (Loki's Castle and Aarhus Bay; Fig. 1a).

To analyse the genomic content and evolutionary history of these novel Asgard lineages, contigs were binned into metagenome-assembled genomes on the basis of their tetra-nucleotide sequence frequencies and DNA sequence coverage patterns across samples

sequences inferred with RAxML and GTRGAMMA model (**c**) showing high support for the phylogenetic affiliation between Asgard archaea and eukaryotes (support values in red). **a–c**, Scale bars indicate number of substitutions per site. Numbers at branches refer to Bayesian posterior probabilities (**b**) and slow non-parametric maximum-likelihood bootstrap values (**c**). Trees were rooted with Euryarchaeota + DPANN (**a**, **b**) and with Bacteria (**c**). Branch length value corresponding to cut branch in **c** is 0.6769. **d**, Schematic tree of Asgard lineages and corresponding overview of identified ESPs. Black circles, ESP predicted based on presence of arCOG, (TopoIB, rpb8, RNA polymerase) or IPR domain (all others); grey circles, putative ESP homologues present; empty circles, no ESP homologue identified (Extended Data Table 2). \*Most Asgard genomes encode distantly related FtsZ homologues (Supplementary Discussion 3).

(Extended Data Fig. 1b, Supplementary Discussion 2). We reconstructed near-complete genome bins for representatives of each major Asgard clade (Fig. 1a, Extended Data Table 1). Analysis of the small subunit rRNA genes identified in these genome bins revealed that Asgard archaea are present in sediments of a wide variety of anaerobic environments (Extended Data Fig. 1c). In contrast to Lokiarchaeota, which are relatively abundant and mostly present in marine sediments, relatives of Heimdall-, Odin- and Thorarchaeota seem to represent low-abundance community members based on 16S rRNA gene surveys (Extended Data Fig. 1c). In accordance with the above-mentioned RP15 analyses, Odinarchaeota seem to be almost exclusively present in high-temperature habitats (97.5% of all available 16S rRNA gene sequences). Moreover, we found that the 16S rRNA sequence of the Heimdallarchaeota genome bin from Aarhus Bay is closely related to the ancient Archaea group (AAG)<sup>24</sup>.

## Asgard archaea and eukaryotes share a common ancestry

To carefully determine the phylogenetic position of the novel Asgard lineages in relation to other Archaea and to eukaryotes, we performed various in-depth phylogenomic analyses of concatenated rRNA gene and conserved marker protein sequence datasets. Resolving the phylogenetic position of such deep evolutionary splits in the tree of life is extremely difficult as the nature of sequence evolution can potentially invoke a number of phylogenetic artefacts<sup>25</sup>. First of all, it is challenging to select appropriate markers since vertically inherited genes shared by evolutionary distantly related lineages are generally limited. Furthermore, while a broad sampling of representative taxa is important, computational feasibility limits the dataset size that can be analysed with current methods. Inclusion of distantly related taxa is known to cause phylogenetic artefacts (such as long branch attraction) and it is therefore important to employ phylogenetic approaches that can adequately account for mutational saturation (resulting in loss of evolutionary signal) and unequal mutation rates across different sites over time and between different taxa (that is, heterotachy and compositional bias, respectively).

To address these challenges, we based our analyses on a carefully selected set of taxa and genetic markers and employed phylogenetic approaches that capture heterogeneity of the evolutionary process<sup>26</sup>, as well as data treatments (amino acid recoding) designed to deal with mutational saturation and model violations (see Methods for details; Supplementary Discussion 3). We performed phylogenomic analyses on three different concatenated datasets, comprising 16S and 23S rRNA genes, universally conserved marker genes, and an extended set of ribosomal (r-) proteins that, in addition to universal r-proteins, includes r-proteins only shared between archaea and eukaryotes. This latter set was used to assess potential artefacts resulting from distant outgroup rooting (Supplementary Discussion 3).

By assessing variations in gene/protein datasets, alignment trimming settings, taxon selection, amino acid recoding, removal of biased positions and phylogenetic inference methods, we determined a robust phylogenetic affiliation between Asgard lineages and eukaryotes (Supplementary Tables 4 and 5). Throughout all analyses Asgard archaea formed a well-supported monophyletic group within archaea that emerged as sister group to the TACK superphylum and comprised four distinct archaeal clades (Fig. 1b, c and Extended Data Fig. 2). We propose a phylum level status for Loki-, Thor-, Odin- and Heimdallarchaeota, and superphylum status for Asgard (Supplementary Table 3, Supplementary Discussion 1). Importantly, our phylogenomic analyses placed eukaryotes inside the Asgard superphylum, with high support for the concatenated r-proteins (posterior probability (PP) = 1; Fig. 1b), and conserved marker proteins (PP = 0.95; Extended Data Fig. 2), as well as for the rRNA gene dataset (bootstrap support (BS) = 91; Fig. 1c). Notably, the majority of the converged (maxdiff < 0.3) Bayesian phylogenetic analyses link eukaryotes to Heimdallarchaeota as the closest branching clade, albeit with insignificant support values (PP = 0.77 in Fig. 1b; BS = 28–42 in Fig. 1c; PP = 0.77 in Extended Data Fig. 2; Supplementary Table 4, Supplementary Discussion 3). Hence, while the phylogenetic affiliation between Asgard archaea and eukaryotes is strong, our analyses failed to resolve the exact position of eukaryotes relative to the Asgard superphylum (either as a sister group or nested within), or the positions of Asgard phyla relative to each other (Supplementary Tables 4–6). Several reasons could potentially explain this lack of phylogenetic resolution, but we suspect that an improved taxon availability of Asgard lineages could further resolve this problem (Supplementary Discussion 3).

## Eukaryotic signatures in Asgard genomes

Next, to gain further insight into the emergence of eukaryotic gene content, we identified potential eukaryotic signature proteins (ESPs) in the reconstructed Asgard genomes. Notably, all Asgard lineages were found to be enriched for such ESPs, suggesting that these are

widespread across the Asgard superphylum (Extended Data Table 2, Supplementary Tables 7 and 8). ESPs identified in the new Asgard genomes previously identified in the composite Lokiarchaeum genome<sup>11,14</sup> included an expanded set of GTPases (Extended Data Fig. 3, Supplementary Table 8), eukaryotic RLC7 family proteins (Supplementary Fig. 1), actin homologues (Supplementary Fig. 2), gelsolin-domain proteins, components of eukaryotic ESCRT (I, II and III) systems including two sub-families of SNF7 proteins (Supplementary Fig. 3), ubiquitin modifier system components (Supplementary Fig. 4) and homologues of eukaryotic protein translocation and glycosylation pathways (Extended Data Table 2, Extended Data Fig. 4). Notably, in the genomes of Heimdallarchaeote AB\_125 and Odinarchaeote LCB\_4, genes encoding ESCRT and ubiquitin modifier system components are co-organized in the same gene cluster (Extended Data Fig. 5). This observation supports the proposal that these systems might be involved in ESCRT-mediated protein degradation<sup>11</sup>, a pathway previously only known in eukaryotes<sup>27</sup>. Yet, the fact that the ubiquitin modifier system is absent from thorarchaeal genomes suggests that these ESCRT proteins could be associated with alternative functions, or that these latter archaea have a different mechanism for cargo recognition.

We identified several new eukaryotic signatures in Asgard lineages that were not previously detected in the composite Lokiarchaeum genome. These newly identified ESPs comprise a functionally diverse set of proteins that generally display a punctuated distribution across Asgard archaea. Remarkably, we identified a bona fide tubulin orthologue in members of the Odinarchaeota (Extended Data Fig. 6a) that is more closely related to eukaryotic tubulins than those previously reported in Thaumarchaeota (artubulins)<sup>28</sup>. This finding, together with the identification of conserved ‘lokiactins’ (Supplementary Fig. 2), gelsolin- and profilin-domain proteins and homologues of subunit 4 of the ARP2/3 complex in different lineages (Extended Data Table 2, Supplementary Table 7, Supplementary Discussion 4), indicates that Asgard archaea contain sophisticated cytoskeletal machineries, with orthologues of key cytoskeletal components in eukaryotes. In addition, the newly identified ESPs include proteins with information processing functions, such as the putative homologues of the ε DNA polymerase subunit (Extended Data Fig. 6b, c) and of ribosomal protein L28e/Mak16 (Extended Data Fig. 6d), both of which were identified in the genome of Heimdallarchaeote LC\_3. While the ε-like DNA polymerase of Heimdallarchaeote LC\_3 represents the closest homologue of eukaryotic ε DNA polymerases found so far and contains one of two characteristic C-terminal zinc-fingers, it lacks a domain of unknown function (PF08490) that is present in all eukaryotic ε DNA polymerases (Extended Data Fig. 6c) and may be derived from an additional inactivated PolB<sup>29</sup> (Supplementary Discussion 4). This suggests that this domain was recruited later in eukaryotic evolution, perhaps after the acquisition of the mitochondrial endosymbiont.

Furthermore, some ESPs previously found in TACK archaea (which are related to Asgard) but absent from the Lokiarchaeum genome, were identified in some Asgard lineages (Fig. 1d), including homologues of the G subunit of the RNA polymerase (Rpb8) in Odinarchaeota and Heimdallarchaeote LC\_3, of topoisomerase IB in Thorarchaeota and of a fused RNA polymerase A in Heimdallarchaeote LC\_3 (but see Supplementary Discussion 4, Supplementary Fig. 5a, b).

## Identification of membrane-trafficking components

Generally, many of the Asgard ESPs were functionally assigned to intracellular trafficking and secretion (Extended Data Fig. 7, Supplementary Discussion 4). A close inspection of these ESPs revealed that Thorarchaeota genomes uniquely encode several homologues of eukaryotic proteins involved in membrane-trafficking processes. We found that each thorarchaeal genome encoded proteins belonging to two orthologous protein families with domain signatures of the eukaryotic TRAPP complex. In eukaryotes, TRAPP complexes represent multi-subunit vesicle-tethering factors that are involved in various trafficking activities, including endoplasmic reticulum to Golgi and

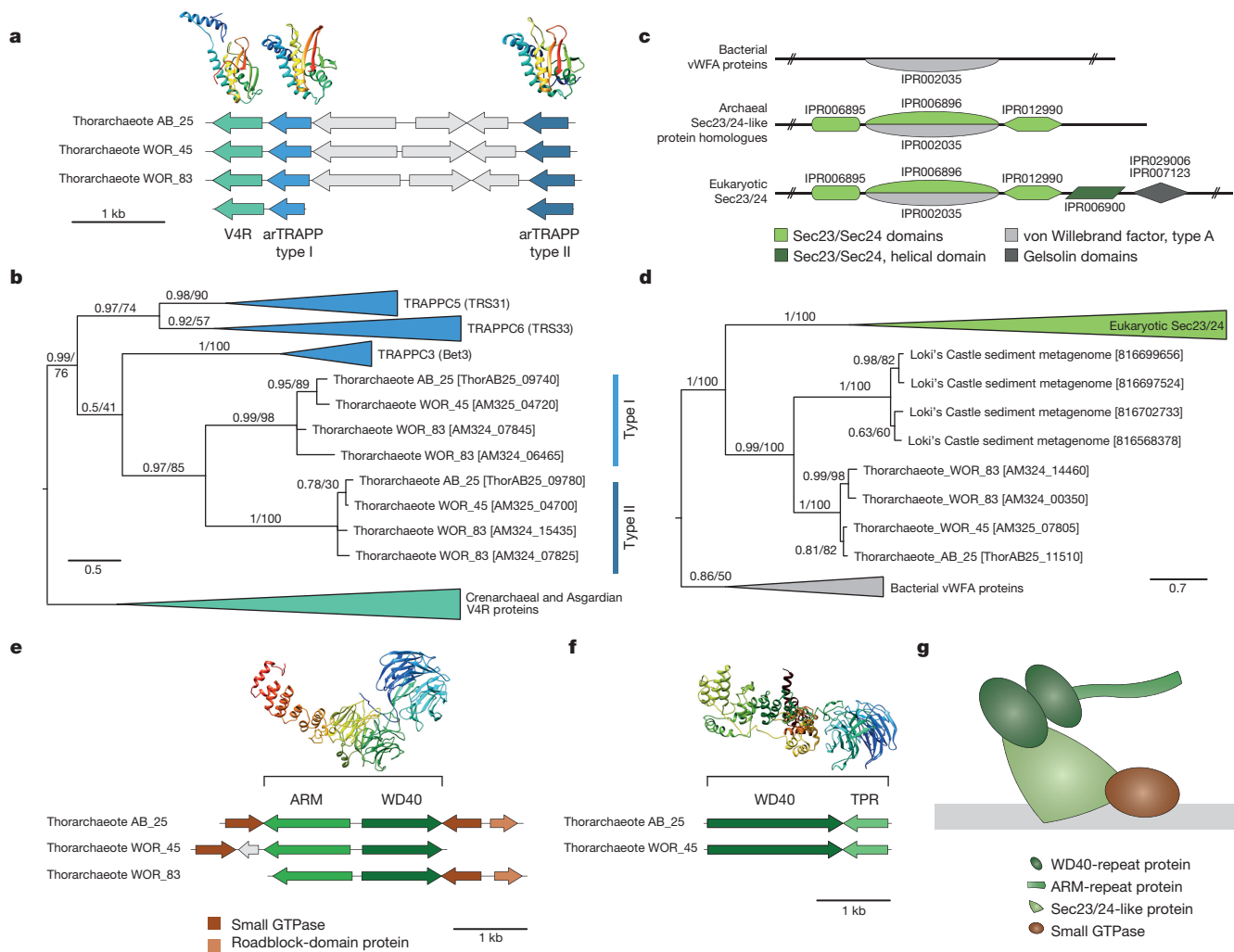


**Figure 2 | Vesicular trafficking components in Asgard archaea.**

**a**, Conserved thorarchaeal gene clusters comprising archaeal (ar) TRAPP- and V4R-domain-encoding genes and corresponding predicted protein models of Thorarchaeote AB\_25 homologues. **b**, Bayesian inference of thorarchaeal Bet3 homologues and subunits of the eukaryotic TRAPP complex. The tree was rooted with crenarchaeal and Asgard V4R-domain proteins. **c**, Domain topology of archaeal and eukaryotic Sec23/24 proteins, and prokaryotic von Willebrand factor proteins. **d**, Bayesian inference of thorarchaeal and metagenomic Sec23/24 homologues that branch basal to eukaryotic Sec23/Sec24 sequences. The tree was rooted with bacterial von Willebrand factor proteins. **e**, Thorarchaeal gene

trans-Golgi transport<sup>30</sup>. The genes encoding thorarchaeal TRAPP domain proteins are part of a gene cluster that also encodes a protein with a more distantly related V4R domain, which is present in both archaeal and bacterial genomes (Fig. 2a). Phylogenetic analyses of the thorarchaeal TRAPP domain proteins revealed that they form a monophyletic group with eukaryotic TRAPPC3 (Bet3 family), TRAPPC5 and TRAPPC6 family proteins. This indicates that the thorarchaeal homologues are more closely related to eukaryotic TRAPP proteins than any of the V4R domain proteins previously detected in prokaryotes, including those of *Lokiarchaeum* and *Ignicoccus hospitalis* (Fig. 2b)<sup>14,31</sup>. These findings, which are also supported by protein structure prediction analyses (Fig. 2a, Supplementary Table 9), underline the archaeal ancestry of eukaryotic TRAPP family proteins C3, C5 and C6<sup>31</sup>.

In addition, thorarchaeal genomes encode homologues of eukaryotic Sec23/24 family proteins, which are essential components of COPII, a protein complex responsible for vesicle-mediated ER-to-Golgi transport of protein cargo<sup>32</sup>. Protein domain and structure prediction analysis of these thorarchaeal Sec23/24 homologues indicate that they

clusters encoding a protein with a predicted β-propeller fold (WD40-repeat protein), an adjacent protein with a predicted α-solenoid fold (ARM-repeat protein), and one or more small GTPases. **f**, Thorarchaeal gene clusters that encode a TPR-domain protein located next to a WD40-repeat protein. **g**, Schematic depiction of a putative archaeal proto-coatomer complex. **a, c, e, f**, Scale bar indicates the number of substitutions per site. Numbers at branches refer to Bayesian (**a**) and slow non-parametric maximum-likelihood bootstrap values (**c**). **b, d, f**, Protein models for Thorarchaeota AB\_25 are shown above the respective genes, with proteins for structures shown in **e** and **f** being artificially fused before modelling (Supplementary Tables 6 and 7).

contain the zinc-finger, trunk and β-sandwich domains of eukaryotic Sec23/24 family proteins, but lack the C-terminal helical and gelsolin domains (Fig. 2c). The basal position of the thorarchaeal Sec23/24 homologues relative to their eukaryotic counterparts in phylogenetic analyses suggests an archaeal ancestry of the eukaryotic proteins (Fig. 2d). During eukaryotic COPII-mediated vesicle biogenesis, Sec23 and Sec24 function as GTPase-activating protein (GAP) and cargo acceptor, respectively, while these functions are mediated by longin domain proteins in other vesicle coats<sup>33</sup>.

The present identification of Sec23/24 domain proteins in all our thorarchaeal genome bins, in addition to the presence of longin domain proteins in *Lokiarchaeota*<sup>11,14</sup> as well as in *Heimdall-* and *Odinarchaeota* (Extended Data Table 2, Fig. 1d) prompted us to search for potential coatomer proteins. Eukaryotic coatomers are characteristically composed of N-terminal β-propeller folds followed by a C-terminal α-solenoid fold. While proteins containing either β-propeller or α-solenoid folds are widespread among prokaryotes<sup>34</sup>, including all Asgard lineages (Supplementary Table 10 and 11),

proteins containing both folds are extremely rare outside the eukaryotic domain<sup>35</sup>. Notably, all three thorarchaeal genomes contain gene clusters that encode a WD40-repeat protein with a predicted  $\beta$ -propeller fold, an adjacent protein with a predicted  $\alpha$ -solenoid domain (armadillo (ARM)-repeat protein), in addition to one or more small GTPases (Fig. 2e). Structure predictions of the concatenated thorarchaeal WD40- and ARM-repeat proteins revealed that these resemble eukaryotic COP  $\alpha$  and  $\beta$  subunits (with 97% of the residues modelled at >90% confidence in Thorarchaeote AB\_25; Supplementary Table 9). According to a recent study,  $\alpha$ -solenoid-fold proteins can be comprised of tetratricopeptide repeats (TPR)<sup>36</sup>. We also identified thorarchaeal gene clusters in which genes encoding a TPR-domain protein and a WD40-repeat protein were located adjacently (Fig. 2f). Notably, the TPR-domain protein shows a significant domain hit to the COP  $\epsilon$  subunit, and, upon concatenation, structural homology to the COP  $\alpha$  subunit was observed (with 87% of the residues modelled at >90% confidence in Thoarchaeote AB\_25; Fig. 2f and Supplementary Table 9). Other WD40-domain proteins detected in Asgard lineages do not seem to be located adjacent to putative  $\alpha$ -solenoid-fold proteins (Supplementary Tables 10 and 11).

The discovery of the basic building blocks of eukaryotic coatomers, archaeal Sec23/24 and TRAPP C3/C5/C6 homologues in addition to the previous detection of longin- and gelsolin-domain proteins as well as a plethora of small GTPases in Asgard lineages<sup>11,14,15</sup>, brings a new perspective on the origin and early evolution of eukaryotic membrane-trafficking machineries. First of all, we demonstrate that several fundamental building blocks for the evolution of a primordial vesicular machinery derive from the archaeological ancestor of eukaryotes rather than from the mitochondrial endosymbiont<sup>34</sup> (Supplementary Discussion 4). Our findings indicate that the origin of the eukaryotic trafficking machinery predates the mitochondrial origin.

Furthermore, our study provides support to the protocoatomer hypothesis<sup>35,37</sup>, which posits that all major eukaryotic membrane deforming complexes evolved from an ancestral proto-coatomer domain architecture comprising  $\beta$ -propeller and  $\alpha$ -solenoid folds<sup>38</sup>. Support for this hypothesis is based on structural homology of subunits of the COP complexes, clathrin adaptor proteins (AP1–5), nuclear pore complex (Sec13/31), intraflagellar transport complex and several less-studied trafficking complexes, such as TSET, SEA and HOPS/CORVET<sup>35</sup>. The presence of  $\beta$ -propeller/ $\alpha$ -solenoid gene clusters in archaea basal to eukaryotes suggests an archaeological provenance of this architecture.

Based on these findings, the last common ancestor of Asgard archaea and eukaryotes could have had the ability to assemble primordial coatomer (Fig. 2g) and ‘proto-TRAPP’ complexes, the latter comprising TRAPP C3/5/6 subunits, longin domain proteins and cognate small GTPases. These early trafficking complexes subsequently evolved by gene fusion (for example, of  $\beta$ -propellers and  $\alpha$ -solenoids) and duplication events in the early stages of eukaryogenesis<sup>39</sup>.

## Discussion and future perspective

In this study, we employed a metagenomics approach to reveal the existence of uncultivated archaeological lineages that are distantly related to the recently described Lokiarchaeota. We have shown that these lineages form a candidate superphylum, designated Asgard archaea, that affiliates robustly with eukaryotes in phylogenetic analyses, and that reconstructed Asgard genomes encode an enriched repertoire of eukaryotic signature proteins. Apart from reinforcing the validity of the two-domain topology of the tree of life and symbiogenic scenarios<sup>17</sup>, the findings reported here provide several new insights into the process of eukaryogenesis. Asgard archaea encode many key components underlying the emergence of eukaryotic cellular complexity, including homologues of eukaryotic proteins involved in cytoskeletal functions and vesicle formation and trafficking (Extended Data Fig. 8). In addition, Asgard genomes seemingly encode a large amount of proteins that are most similar to bacterial proteins, which may explain some of the bacterial genes present in eukaryotic genomes<sup>40–42</sup>. Altogether, this

indicates that the genetic repertoire of the archaeological ancestor of eukaryotes was more complex than anticipated previously<sup>43</sup>.

Yet what do these findings tell us about the level of cellular complexity of the Asgard lineages, and, by inference, of the last archaeo-eukaryotic common ancestor (LAECA)? As the phylogenetic and comparative analyses presented here do not allow us to pinpoint the molecular functions of these ESPs, experimental verification is needed to assess whether these proteins are functionally equivalent to their presumed eukaryotic counterparts. LAECA, however, lived around 2 billion years ago, in a world that was very different from what we observe today, and cell biological research on Asgard archaea might therefore hold limited relevance for inferring cellular characteristics of LAECA. Assuming that all ESPs currently identified in various Asgard lineages were present in LAECA and functionally equivalent to their eukaryotic homologues, how ‘eukaryotic’ was this ancestor in terms of its cellular complexity? In the prokaryotic world, the ability to form both extracellular and intracellular membrane structures and/or compartments is by no means exceptional. Many bacterial lineages are known to sustain internal membrane structures (for example, thylakoids in cyanobacteria, magnetosomes in magnetotactic bacteria, power-generating membranes in various nitrifying and methylotrophic bacteria, membrane structures of unknown function in Planctomycetes; reviewed in ref. 44). Notably, the crenarchaeon *Ignicoccus hospitalis* has the ability to form ‘intermembrane’ vesicles that are thought to mediate transport between its unusual inner and outer membranes<sup>45</sup>. Moreover, the presence of two membranes has recently also been confirmed in other archaeological lineages (reviewed in ref. 46). As such, and given the observed sets of ESPs in Asgard genomes, it seems therefore possible that members of the Asgard archaea (and LAECA) have (had) the ability to bend membranes and to form and transport internal vesicles, albeit at a much more primitive level than observed in modern eukaryotes.

The central question with regard to eukaryogenesis entails, however, why a particular Asgard lineage evolved the far higher level of cellular complexity characteristic of eukaryotes, whereas other prokaryotic lineages did not. The genomic repertoire of Asgard archaea suggests that mitochondria were acquired after the invention of several fundamental building blocks for the evolution of complex eukaryotic features. While these findings may suggest the ability of simple phagocytic capabilities in the archaeological host<sup>17,47–49</sup>, the exact time point and mechanism of symbiont acquisition require further investigation<sup>2</sup>. Nevertheless, in line with many symbiogenic hypotheses<sup>3,4</sup>, we believe that the driving force behind the increase in complexity seen in eukaryotic cells has been the acquisition of the mitochondrial endosymbiont. The uncoupling of energy production from the host cell’s external membrane to the mitochondrial inner membrane as well as the increase of energy availability allowed the increase in cell size and volume<sup>50</sup>, and evolution of more complex and energy-demanding cellular structures, including sophisticated endomembrane systems, the nucleus and fully-fledged endocytic and phagocytic machineries. The emergence of such capabilities was an essential step in the evolution of eukaryotes.

Future exploration of novel branches in the tree of life, including novel members of the Asgard, as well as deep-branching eukaryotes, and the detailed characterization of their metabolic repertoires and cell-biological features, will undoubtedly provide new fundamental insights into the process of eukaryogenesis, and ultimately reveal how eukaryotic cells evolved their complex and compartmentalized nature.

**Online Content** Methods, along with any additional Extended Data display items and Source Data, are available in the online version of the paper; references unique to these sections appear only in the online paper.

Received 30 June; accepted 2 December 2016.

Published online 11 January 2017.

- Embley, T. M. & Martin, W. Eukaryotic evolution, changes and challenges. *Nature* **440**, 623–630 (2006).
- López-García, P. & Moreira, D. Open questions on the origin of eukaryotes. *Trends Ecol. Evol.* **30**, 697–708 (2015).

3. Koonin, E. V. Origin of eukaryotes from within Archaea, archaeal eukaryome and bursts of gene gain: eukaryogenesis just made easier? *Phil. Trans. R. Soc. Lond. B* **370**, 20140333 (2015).
4. Martin, W. F., Garg, S. & Zimorski, V. Endosymbiotic theories for eukaryote origin. *Phil. Trans. R. Soc. Lond. B* **370**, 20140330 (2015).
5. Cox, C. J., Foster, P. G., Hirt, R. P., Harris, S. R. & Embley, T. M. The archaeabacterial origin of eukaryotes. *Proc. Natl Acad. Sci. USA* **105**, 20356–20361 (2008).
6. Guy, L. & Ettema, T. J. The archaeal ‘TACK’ superphylum and the origin of eukaryotes. *Trends Microbiol.* **19**, 580–587 (2011).
7. Raymann, K., Brochier-Armanet, C. & Gribaldo, S. The two-domain tree of life is linked to a new root for the Archaea. *Proc. Natl Acad. Sci. USA* **112**, 6670–6675 (2015).
8. McInerney, J. O., O’Connell, M. J. & Pisani, D. The hybrid nature of the Eukaryota and a consilient view of life on Earth. *Nat. Rev. Microbiol.* **12**, 449–455 (2014).
9. Williams, T. A., Foster, P. G., Nye, T. M., Cox, C. J. & Embley, T. M. A congruent phylogenomic signal places eukaryotes within the Archaea. *Proc. R. Soc. Lond. B* **279**, 4870–4879 (2012).
10. Gray, M. W., Burger, G. & Lang, B. F. Mitochondrial evolution. *Science* **283**, 1476–1481 (1999).
11. Spang, A. et al. Complex Archaea that bridge the gap between prokaryotes and eukaryotes. *Nature* **521**, 173–179 (2015).
12. Williams, T. A., Foster, P. G., Cox, C. J. & Embley, T. M. An archaeal origin of eukaryotes supports only two primary domains of life. *Nature* **504**, 231–236 (2013).
13. Hartman, H. & Fedorov, A. The origin of the eukaryotic cell: a genomic investigation. *Proc. Natl Acad. Sci. USA* **99**, 1420–1425 (2002).
14. Klinger, C. M., Spang, A., Dacks, J. B. & Ettema, T. J. Tracing the archaeal origins of eukaryotic membrane-trafficking system building blocks. *Mol. Biol. Evol.* **33**, 1528–1541 (2016).
15. Surkort, J. & Pereira-Leal, J. B. Are there Rab GTPases in Archaea? *Mol. Biol. Evol.* **33**, 1833–1842 (2016).
16. Dey, G., Thattai, M. & Baum, B. On the archaeal origins of eukaryotes and the challenges of inferring phenotype from genotype. *Trends Cell Biol.* **26**, 476–485 (2016).
17. Koonin, E. V. Archaeal ancestors of eukaryotes: not so elusive any more. *BMC Biol.* **13**, 84 (2015).
18. Archibald, J. M. Endosymbiosis and eukaryotic cell evolution. *Curr. Biol.* **25**, R911–R921 (2015).
19. Martin, W. F., Neukirchen, S., Zimorski, V., Gould, S. B. & Sousa, F. L. Energy for two: new archaeal lineages and the origin of mitochondria. *BioEssays* **38**, 850–856 (2016).
20. Villanueva, L., Schouten, S. & Damsté, J. S. Phylogenomic analysis of lipid biosynthetic genes of Archaea shed light on the ‘lipid divide’. *Environ. Microbiol.* (2016).
21. Sousa, F. L., Neukirchen, S., Allen, J. F., Lane, N. & Martin, W. F. Lokiarchaeon is hydrogen dependent. *Nat. Microbiol.* **1**, 16034 (2016).
22. Mariotti, M. et al. Lokiarchaeota marks the transition between the archaeal and eukaryotic selenocysteine encoding systems. *Mol. Biol. Evol.* **33**, 2441–2453 (2016).
23. Seitz, K. W., Lazar, C. S., Hinrichs, K. U., Teske, A. P. & Baker, B. J. Genomic reconstruction of a novel, deeply branched sediment archaeal phylum with pathways for acetogenesis and sulfur reduction. *ISME J.* **10**, 1696–1705 (2016).
24. Takai, K. & Horikoshi, K. Genetic diversity of Archaea in deep-sea hydrothermal vent environments. *Genetics* **152**, 1285–1297 (1999).
25. Delsuc, F., Brinkmann, H. & Philippe, H. Phylogenomics and the reconstruction of the tree of life. *Nat. Rev. Genet.* **6**, 361–375 (2005).
26. Lartillot, N. & Philippe, H. A Bayesian mixture model for across-site heterogeneities in the amino-acid replacement process. *Mol. Biol. Evol.* **21**, 1095–1109 (2004).
27. Raiborg, C. & Stenmark, H. The ESCRT machinery in endosomal sorting of ubiquitylated membrane proteins. *Nature* **458**, 445–452 (2009).
28. Yutin, N. & Koonin, E. V. Archaeal origin of tubulin. *Biol. Direct* **7**, 10 (2012).
29. Tahirov, T. H., Makarova, K. S., Rogozin, I. B., Pavlov, Y. I. & Koonin, E. V. Evolution of DNA polymerases: an inactivated polymerase-exonuclease module in Pol epsilon and a chimeric origin of eukaryotic polymerases from two classes of archaeal ancestors. *Biol. Direct* **4**, 11 (2009).
30. Sacher, M., Kim, Y. G., Lavie, A., Oh, B. H. & Segev, N. The TRAPP complex: insights into its architecture and function. *Traffic* **9**, 2032–2042 (2008).
31. Podar, M., Wall, M. A., Makarova, K. S. & Koonin, E. V. The prokaryotic V4R domain is the likely ancestor of a key component of the eukaryotic vesicle transport system. *Biol. Direct* **3**, 2 (2008).
32. Barlowe, C. et al. COPII: a membrane coat formed by Sec proteins that drive vesicle budding from the endoplasmic reticulum. *Cell* **77**, 895–907 (1994).
33. Lee, M. C., Miller, E. A., Goldberg, J., Orci, L. & Schekman, R. Bi-directional protein transport between the ER and Golgi. *Annu. Rev. Cell Dev. Biol.* **20**, 87–123 (2004).
34. Gould, S. B., Garg, S. G. & Martin, W. F. Bacterial vesicle secretion and the evolutionary origin of the eukaryotic endomembrane system. *Trends Microbiol.* **24**, 525–534 (2016).
35. Devos, D. et al. Components of coated vesicles and nuclear pore complexes share a common molecular architecture. *PLoS Biol.* **2**, e380 (2004).
36. Fournier, D. et al. Functional and genomic analyses of alpha-solenoid proteins. *PLoS One* **8**, e79894 (2013).
37. Field, M. C., Sali, A. & Rout, M. P. Evolution: on a bender–BARs, ESCRTs, COPs, and finally getting your coat. *J. Cell Biol.* **193**, 963–972 (2011).
38. Schlacht, A. & Dacks, J. B. Unexpected ancient paralogs and an evolutionary model for the COPII coat complex. *Genome Biol. Evol.* **7**, 1098–1109 (2015).
39. Dacks, J. B. & Field, M. C. Evolution of the eukaryotic membrane-trafficking system: origin, tempo and mode. *J. Cell Sci.* **120**, 2977–2985 (2007).
40. Ku, C. et al. Endosymbiotic origin and differential loss of eukaryotic genes. *Nature* **524**, 427–432 (2015).
41. Pittis, A. A. & Gabaldón, T. Late acquisition of mitochondria by a host with chimaeric prokaryotic ancestry. *Nature* **531**, 101–104 (2016).
42. Ettema, T. J. Evolution: mitochondria in the second act. *Nature* **531**, 39–40 (2016).
43. Koonin, E. V. & Yutin, N. The dispersed archaeal eukaryome and the complex archaeal ancestor of eukaryotes. *Cold Spring Harb. Perspect. Biol.* **6**, a016188 (2014).
44. Shively, J. M. in *Complex Intracellular Structures in Prokaryotes* (ed. Jessup M. Shively) 3–22 (Springer Berlin Heidelberg, 2006).
45. Küper, U., Meyer, C., Müller, V., Rachel, R. & Huber, H. Energized outer membrane and spatial separation of metabolic processes in the hyperthermophilic archaeon *Ignicoccus hospitalis*. *Proc. Natl Acad. Sci. USA* **107**, 3152–3156 (2010).
46. Klingl, A. S-layer and cytoplasmic membrane—exceptions from the typical archaeal cell wall with a focus on double membranes. *Front. Microbiol.* **5**, 624 (2014).
47. Yutin, N., Wolf, M. Y., Wolf, Y. I. & Koonin, E. V. The origins of phagocytosis and eukaryogenesis. *Biol. Direct* **4**, 9 (2009).
48. Martijn, J. & Ettema, T. J. From archaeon to eukaryote: the evolutionary dark ages of the eukaryotic cell. *Biochem. Soc. Trans.* **41**, 451–457 (2013).
49. Poole, A. M. & Gribaldo, S. Eukaryotic origins: how and when was the mitochondrion acquired? *Cold Spring Harb. Perspect. Biol.* **6**, a015990 (2014).
50. Lane, N. & Martin, W. The energetics of genome complexity. *Nature* **467**, 929–934 (2010).

**Supplementary Information** is available in the online version of the paper.

**Acknowledgements** We thank L. Guy, S. L. Jørgensen, T. Williams, N. Lartillot, B. Quang Minh and J. Dacks for useful advice and discussions. We are grateful to D. R. Colman and C. Takacs-Vesbach for collecting the YNP sediment samples under permit #YELL-2010-SCI-5344, to the Japan Agency for Marine-Earth Science & Technology (JAMSTEC) for taking sediment samples from the Taketomi shallow submarine hydrothermal system, and to the Ngāti Tahu Ngāti Whaoa Runanga Trust for their enthusiasm for our research, and assistance in access and sampling of the Ngatamariki geothermal features. We acknowledge the Yellowstone Center for Resources for their assistance and for facilitating this research. We thank A. Simpson for suggesting the name ‘Heimdallarchaeota’. Sequencing of the White Oak River and Colorado River sediment metagenomes was conducted at the Joint Genome Institute, a US Department of Energy Office of Science User Facility, via the Community Science Program. The remaining metagenomes were sequenced at the National Genomics Infrastructure sequencing platforms at the Science for Life Laboratory at Uppsala University, a national infrastructure supported by the Swedish Research Council (VR-RFI) and the Knut and Alice Wallenberg Foundation. We thank the Uppsala Multidisciplinary Center for Advanced Computational Science (UPPMAX) at Uppsala University and the Swedish National Infrastructure for Computing (SNIC) at the PDC Center for High-Performance Computing for providing computational resources. This work was supported by grants of the European Research Council (ERC Starting grant 310039-PUZZLE\_CELL), the Swedish Foundation for Strategic Research (SSF-FFL5) and the Swedish Research Council (VR grant 2015-04959) to T.J.G.E., by Marie Curie IIF (331291 to J.H.S.) and IEF (625521 to A.S.) grants by the European Union to the Ettema laboratory, by grants to Bo Barker Jørgensen (Aarhus University, Denmark) from the European Research Council (ERC Advanced Grant 294200-MICROENERGY) and the Danish National Research Foundation (DNRF104) to support the Center for Geomicrobiology at Aarhus University, and by the US Department of Energy (Sustainable Systems Scientific Focus Area grant DE-AC02-05CH11231 to J.F.B.).

**Author Contributions** T.J.G.E. conceived the study. A.Sc., P.S., K.U.K., M.B.S. and T.N. took/provided environmental samples. L.J. purified environmental DNA and prepared sequencing libraries. K.Z.-N., E.F.C., J.H.S., K.A., J.F.B., K.W.S., B.J.B. and E.V. performed metagenomic sequence assemblies and metagenomic binning analyses. K.Z.-N., E.F.C., J.H.S., A.Sp. and T.J.G.E. analysed genomic data and performed phylogenetic analyses. A.Sp., D.B., E.F.C. and T.J.G.E. analysed genomic signatures. K.Z.-N., E.F.C., J.H.S., A.Sp. and T.J.G.E. wrote, and all authors edited and approved, the manuscript.

**Author Information** Reprints and permissions information is available at [www.nature.com/reprints](http://www.nature.com/reprints). The authors declare no competing financial interests. Readers are welcome to comment on the online version of the paper. Correspondence and requests for materials should be addressed to T.J.G.E. (thijs.etterma@icm.uu.se).

**Reviewer Information** *Nature* thanks J. Gilbert, E. Koonin, A. Roger and the other anonymous reviewer(s) for their contribution to the peer review of this work.

## METHODS

No statistical methods were used to predetermine sample size.

**Sample acquisition.** Metagenomic samples were obtained from the following locations: AB (Aarhus Bay, Denmark), LC (Loki's Castle hydrothermal vent field)<sup>51</sup>, LCB (Lower Culex Basin, Yellowstone National Park, USA)<sup>52</sup>, RP (Radiata Pool, Ngatamariki, New Zealand), WOR (White Oak River estuary, USA)<sup>23</sup>, CR (aquifer near Colorado River, USA)<sup>53</sup>, and TIV (Taketomi Island shallow submarine hydrothermal field, Japan)<sup>54</sup>. Four sediment samples from AB were retrieved from gravity cores at station M5 and at depths (0.25, 0.75, 1.25 and 1.75 m below sea floor). Subsamples were taken from the original core samples using sterile, cut-off 5-ml syringes less than 4 h after retrieval and stored at -80°C until further processing. Sediment from TIV was taken by a push corer with scuba diving. The sediment cores were sectioned every 5 cm, and stored at -80°C and -25°C. The GPS coordinates of the locations from which samples were obtained are: AB (56° 06' 12" N, 10° 27' 28.2" E), LC (73° 45' 47.4" N, 8° 27' 50.4" E), RP (38° 31' 48.0" S, 176° 10' 12.0" E), LCB (44° 34' 23.0" N, 110° 47' 40.5" W), WOR (34° 44' 35.5" N, 77° 07' 26.1" W), CR (39° 31' 44.69" N, 107° 46' 19.71" W), and TIV (24° 20' 54.0" N, 124° 06' 06.0" E).

**DNA extraction and sequencing.** Detailed descriptions of DNA extraction, metagenomic library preparation, and sequencing for LC, LCB, WOR and CR samples have been provided as part of previous studies<sup>23,51-53</sup>. DNA from TIV sediment sample 617-1-3 was extracted from approximately 10 g of sediment material using Power Max Soil DNA isolation kit (MoBio Labs) following manufacturer's instructions. The extracted DNA in 5 ml of water was purified using the Aurora system (Boreal Genomics) to remove potential inhibitors. DNA from RP hot spring sample P1.0019 was extracted from approximately 10 g of sediment material using FastDNA 50 ml spin kit for soil (MP Biomedicals) spiked with 400 µl of PolyA (10 ng µl<sup>-1</sup>; Sigma-Aldrich). The DNA eluted in 5 ml of water was further cleaned using the Aurora system. DNA concentrations at various stages of extraction and library construction were measured with ND-3300 fluorescent Nanodrop instrument (Thermo Scientific). DNA from AB samples was extracted using two methods: a protocol established by Lever *et al.*<sup>55</sup> abbreviated as MM, and by PowerMax Soil DNA Isolation Kit (MoBio Labs; abbreviated as PM) to enable differential coverage binning further downstream. DNA was extracted from approximately 5 g of sediment materials for each of the samples, resulting in eight different DNA extractions for metagenomic sequencing: MM1/PM1, MM2/PM2, MM3/PM3, and MM4/PM4.

Metagenomic sequencing libraries for AB, RP, and TIV samples were prepared from 50 ng, 50 ng, and 1 ng of purified DNA, respectively. Nextera DNA library preparation kit was used for AB and RP samples and Nextera XT DNA library preparation kit was used for the TIV sample. Metagenomic sequence data for AB, TIV, and RP samples was generated with Illumina HiSeq 2000 and HiSeq 2500 instruments at Uppsala SNP&SEQ Technology Platform. The amount of total raw sequence data generated for the metagenomes was: AB (8 samples, 211 Gbp, 2 × 150 or 2 × 250 bp), TIV (1 sample, 49 Gb, 2 × 250 bp), and RP (1 sample, 33 Gb, 2 × 150 bp). Additional sequences for LC sample were generated from the same MDA-treated library from the previous study<sup>51</sup> resulting in a total of 232 Gb of combined sequence data from five separate sequencing runs.

**Abundance and distribution of the Asgard members.** Silva and NCBI nucleotide databases were searched by BLASTN for positive hits to the Asgard members (*E* value cut-off of  $1 \times 10^{-5}$ ) and accession numbers of hits were retrieved to identify their sources of isolation. A custom Python script was used to tabulate the results and to calculate their abundance and distribution.

**Metagenome assembly and binning.** Preprocessing of raw Illumina sequences to remove adaptor sequences and poor-quality regions was carried out using a combination of the following tools: Trimmomatic<sup>56</sup>, Scythe (<https://github.com/vsbuffalo/scythe>), and Sickle (<https://github.com/najoshi/sickle>). Detailed parameters used with the trimming tools are described in the Supplementary Methods. Metagenomic sequences were assembled with either IDBA-UD<sup>57</sup> (AB, CR, RP, TIV, WOR, and LCB) or Ray Meta<sup>58</sup> (LC) assemblers. With the exception of AB samples, all the metagenomes were assembled individually. For the AB samples, MM1 and PM1 metagenomes were co-assembled and PM3 was assembled separately.

Binning of the metagenomic assemblies was done with a combination of the following methods and tools: emergent self-organizing maps (ESOM)<sup>59</sup>, CONCOCT<sup>60</sup>, PhymmBL<sup>61</sup>, ABAWACA<sup>62</sup>, and multi-metagenome<sup>63</sup>. Details on the assembly and binning of Thorarchaeotes WOR\_45 and WOR\_83 have been described previously<sup>23</sup>. All bins were subjected to careful individual contamination removal and quality assessment procedures as described in the Supplementary Methods. In brief, Thorarchaeote AB\_25 genome bin was extracted from the MM1/PM1 co-assembly by first using CONCOCT and by further manually cleaning the initial bin using mmgenome tool<sup>63</sup>. Heimdallarchaeote AB\_125 genome bin from PM3 was identified through two rounds of ESOM binning, setting the minimum

nucleotide fragment length to 10 kb in the first round and 5 kb in the second round and also further manually cleaned using mmgenome tool. Odinarchaeote LCB\_4 genome bin was first extracted from YNP metagenome by ESOM binning and subsequently read pairs mapped to the contigs assigned to the bin were reassembled using SPAdes<sup>64</sup> (version 3.5.0). The metagenomic contigs from CR sample were initially binned using the ABAWACA tool<sup>62</sup> and contigs that could not be assigned to any cluster assigned by ABAWACA were binned using ESOM. Lokiarchaeote CR\_4 came from a cluster binned using ESOM. Heimdallarchaeota LC\_2 and LC\_3 were extracted from the LC sample using both PhymmBL and ESOM binning, by taking the intersection of contigs identified by these two independent methods. Further cleaning was performed using coverage information from the unamplified metagenome. The three marine Korarchaeotes were extracted from the TIV metagenome using ESOM binning (see Supplementary Methods for details). Completeness, contamination, and strain heterogeneity of all the genome bins were assessed using CheckM<sup>65</sup> and micomplete<sup>51</sup> tools.

**Annotation of genome bins.** Coding sequences were identified using Prodigal<sup>66</sup> using '-p single' option for Odinarchaeote LCB\_4, '-m -p meta' for Lokiarchaeote CR\_4, or '-p meta' option for all other genomic bins. Genes of Thorarchaeotes WOR\_45 and WOR\_82 bins were predicted using the JGI IMG/MER system<sup>23,67</sup>. Ribosomal RNA-coding regions (16S, 23S, 5S) and transfer RNA-coding regions were predicted with Barrnap (<https://github.com/tseemann/barrnap>) and tRNAscan-SE<sup>68</sup>, respectively. All proteomes were queried against nr (using NCBI database as of February 2015) and protein domains were determined using InterProScan<sup>69</sup> with default parameters and RPS-BLAST against the NCBI CDD database<sup>70</sup>. Furthermore, all proteins were assigned to existing arCOGs<sup>71</sup> (archaeal cluster of orthologous groups), while new arCOGs were generated as described previously<sup>51</sup>. Potential ESPs were identified by determining all Asgard proteins that retrieved hits to eukaryote-specific IPR domains (see Extended Data Table 2, Supplementary Tables 7 and 8). Several of these ESPs, were further investigated using PFAM<sup>72</sup>, SMART<sup>73</sup> and Hmmpred<sup>74</sup> for remote homology detection, the protein structure prediction tool Phyre2<sup>75</sup> for homology modelling and through phylogenetic analyses (see single gene phylogenies in Supplementary Information). Predicted models were viewed and analysed further using Chimera<sup>76</sup> (Supplementary Tables 9 and 10).

**Comparison of full length 16S sequences.** 16S identities were calculated using needle (-gapopen 10 -gapextend 0.5) for each pair of full-length 16S sequences (Heimdallarchaeote AB\_125, Heimdallarchaeote LC\_3, Odinarchaeote LCB\_4, Odinarchaeote RP\_19, Lokiarchaeote CR\_4, Lokiarchaeum and Thorarchaeote WOR\_83). In the case of Thorarchaeote WOR\_83, long unaligned regions were excluded from the calculation (positions 815–1,558 and 1,746–1,799 removed).

**Phylogenomic analysis using concatenated ribosomal proteins to assess the diversity of Asgard in metagenomes.** A custom pipeline written in Python was used to identify r-protein-containing contigs in all the metagenomes analysed in this study. Briefly, the pipeline uses PSI-BLAST to search for a set of 15 syntenic r-proteins that occur on a single contig given a minimum cutoff of 6 proteins. The set of r-proteins (L2, L3, L4, L5, L6P, L14, L15, L18, L22, L24, S3, S8, S10, S17, and S19) was chosen according to Castelle *et al.*<sup>53</sup>. All identified r-proteins were then aligned individually, trimmed with trimAl and concatenated. RAxML<sup>77</sup> (version 8.1.17) with fast bootstrapping was used to infer maximum likelihood phylogenies, using the PROTCATLG model of protein evolution.

**Identification of taxonomic marker genes.** Taxonomic marker genes used for concatenated phylogenetic analyses were identified as described previously<sup>51,78</sup>. Single-gene RAxML phylogenies were performed for all those markers to assess contamination and suitability for inclusion in concatenated data set. This yielded a final data set of 48 single-copy marker genes. The full list of marker genes selected for phylogenomic analyses is shown in Supplementary Table 9 and includes 31 universal ribosomal proteins (r-proteins). Additional 25 r-proteins shared between Archaea and Eukarya and universally present among Archaea were identified through arCOGs based on Yutin *et al.*<sup>79</sup> to generate a ribosomal protein data set (Supplementary Table 13). Asgard proteins that were classified into ribosomal arCOGs were aligned and end-trimmed to create HMM profiles. Bins were translated into six reading frames and HMMsearch was performed using Asgard-specific ribosomal profiles to retrieve missing ribosomal proteins from Asgard proteomes. Eukaryotic copies of the r-proteins were identified by PSI-BLAST with an *E* value threshold of  $1 \times 10^{-6}$ . Single gene RAxML phylogenies were performed to verify the selection of the eukaryotic copies.

**Phylogenomic analyses of concatenated protein datasets.** Taxa included in this analysis were selected carefully to yield a representative set of Archaea, Bacteria and Eukarya. Each of the 48 single-copy marker genes (from Eukarya, Bacteria and Archaea) as well as the 55 ribosomal proteins (from Archaea and Eukarya) were aligned using MAFFT-L-INS-I<sup>80</sup>, manually inspected and edited to trim the beginning and end of alignments. Further trimming was performed using using

BMGE<sup>81</sup> using the BLOSUM30 matrix or trimAl<sup>82</sup> using the 'gappyout' option. Final alignments for each of the two gene sets were generated by concatenating the 48 marker genes and the 55 ribosomal proteins, respectively. Bayesian inference phylogenies were inferred using PhyloBayes<sup>83</sup> MPI 1.5a, using the CAT-GTR model. Four chains were run in parallel until topological convergence and half of the generations were regarded as burn-in and removed to obtain the summaries for all runs (Supplementary Table 4 and Supplementary Methods). Maximum likelihood phylogenies were inferred using IQ-TREE<sup>84</sup> with mixture models (see Supplementary Methods for details) with ultrafast bootstrapping<sup>85</sup>, as well as the Shimodaira–Hasegawa-like approximate likelihood-ratio test<sup>86</sup>.

To test robustness of the phylogenies, the two data sets were subjected to several treatments and tests. First, influence of the alignment filtering treatment was assessed by comparing alignments trimmed with BMGE<sup>81</sup> and trimAl<sup>82</sup>, as well as with and without manual end-trimming. In addition, taxon removal was used to assess the robustness of the placement of eukaryotes, for example, by removing DPANN Archaea and Bacteria in case of the universal markers concatenation. Posterior predictive tests were performed using PhyloBayes<sup>83</sup> (-comp option) to detect violation of the assumption of homogenous composition. The test statistic calculates maximum square deviation between taxa and the global empirical frequencies and the value observed for the data are compared to the posterior distribution giving z-scores and P values (Supplementary Table 4). Taxa identified as most compositionally biased<sup>87</sup> were removed (Supplementary Table 14 and Supplementary Methods for all the numbers and the list of removed taxa) and yielded a non-biased dataset that included all of the Asgard lineages. Further, eukaryotes were removed to reconstruct the relationships within Asgard. Finally, SR4-recoding was used to evaluate potential biases coming from model mis-specification and saturation of the phylogenetic signal<sup>88</sup>.

**Phylogenomic analysis using concatenated ribosomal RNA genes.** Small subunit (SSU) and large subunit (LSU) ribosomal RNA (rRNA) genes from representative archaeal clades were aligned together with those from Asgard lineages using MAFFT-L-INS-i, trimmed with BMGE and concatenated. Heimdallarchaeote LC\_2 genome bin lacks the SSU rRNA but has a partial LSU rRNA gene and was included in the alignment. Maximum-likelihood phylogenetic analyses were performed using RAxML<sup>77</sup> v.8.0.22, calculating 100 non-parametric bootstraps and using the GTRGAMMA model of sequence evolution and Bayesian inference was carried out with PhyloBayes<sup>83</sup> MPI (v.1.5a) using CAT-GTR model until convergence was reached between at least two independent chains with a 'maxdiff' below 0.3. Several lineages such as the members of DPANN (Diapherotrites, Parvarchaeota, Aenigmarchaeota, Nanoarchaeota, Nanohaloarchaeota, Woesearchaeota, and Pacearchaeota) and *Methanopyrus kandleri* were excluded in the analyses shown in Fig. 1c to prevent potential phylogenetic artefacts. However, taxon sampling experiments were also constructed with and without Bacteria, DPANN members and eukaryotes to check the robustness of Asgard clade and the affiliation between Asgard members and eukaryotes.

**Phylogenetic analyses of selected eukaryotic signature proteins.** Sec23/24 and TRAPP. Eukaryotic Sec23 and Sec24 homologues are composed of several characteristic IPR domains (Fig. 2c), including zinc-finger (IPR006895), von Willebrand factor (vWF) (IPR002035) and a Sec23/24 β-sandwich (IPR012990) domains. Thorarchaeal proteins were identified that contained these domains and that displayed similarity to eukaryotic Sec23/24 proteins (Supplementary Table 4). No other archaeal or bacterial sequences containing both IPR006895 and IPR002035 domains were found. Taxonomically representative sets of eukaryotic putative Sec23/24 and Sec23/24-like sequences with domain hits to IPR006895, IPR006896/ IPR002035 and IPR012990, were retrieved from UniProt. Furthermore, additional Asgard and metagenomic homologues with domain hits to at least IPR006895 and IPR002035 were added to this dataset. Three bacterial von Willebrand factor proteins with the IPR002035 domain were identified using thorarchaeal sequences as queries against nr (excluding eukaryotes) and included as outgroup. Pairwise comparisons of bacterial and thorarchaeal vWF domain proteins with human Sec23 and Sec24 homologues, respectively, revealed that only thorarchaeal homologues displayed significant similarity to eukaryotic sequences. For instance, while E values for the homology between human Sec24 and Sec23 and Thorarchaeote AB25 (ThorAB25\_11510) were  $7 \times 10^{-11}$  and  $4 \times 10^{-4}$ , respectively, they were only 0.13 and 4.1 for Chryseobacterium (WP\_055983045). Therefore, thorarchaeal homologues seemed to be intermediate between bacterial homologues and eukaryotic Sec23/24 domain proteins and the bacterial sequences were used to root this phylogeny.

Sequences with domain hits to the transport protein particle component (IPR007194) were downloaded from a taxonomically representative set of eukaryotes, including homologues of the three Bet3-like subfamilies: TRAPPC3 (Bet3), TRAPPC5 and TRAPPC6. Prokaryotic proteins containing significant hits to IPR007194 (that is, *Ignicoccus hospitalis*, A8AC56) as well as all Asgard

proteins with domain hits to IPR007194 were added to this dataset. Homologous V4R domain proteins (IPR024096) from Crenarchaeota and Asgard members were included as outgroup.

Sequence sets including V4R/TRAPP and vWF/Sec23/24 homologues, were aligned using MAFFT-L-INS-i<sup>80</sup> version 7 with default parameters. After removal of poorly aligned ends, alignments were trimmed using trimAl<sup>82</sup> with the gappyout option yielding 470 (Sec23/24) and 146 (TRAPP) positions, respectively. Subsequently, trimmed alignments were subjected to maximum likelihood and Bayesian phylogenetic inferences. RAxML<sup>77</sup> v.8.0.22 analyses were run under the GAMMA-LG model (generating ten independent trees for optimization) and 100 non-parametric bootstrap replicates were generated. PhyloBayes<sup>83</sup> MPI 1.5 was run using the CAT-GTR model of protein evolution. Four chains were run in parallel until the 'maxdiff' was below 0.15 and consensus trees were obtained discarding 20% of the generations as burn-in. RAxML bootstrap values were mapped onto the PhyloBayes topologies using the sumtrees program, which is part of the DendroPy package<sup>89</sup>.

**Tubulins.** All tubulin sequences (Interpro accession number IPR000217) were downloaded from the UniProt database, resulting in a dataset comprising 33,296 Eukarya, 22 Bacteria, 9 Archaea, and 4 unclassified sequences. This dataset was further separated into alpha, beta, gamma, delta, epsilon, theta, and cryptic tubulins for Eukarya and reduced to 198 sequences after removal of near-identical sequences and FtsZ homologues. Odinarchaeal tubulin sequences along with the selected homologues were aligned using MAFFT-L-INS-i<sup>80</sup>, manually end-trimmed, and further trimmed using trimAl<sup>82</sup> with gappyout option yielding a final alignment of 446 amino acids. Maximum likelihood phylogenetic tree was inferred using RAxML<sup>77</sup> v.8.0.22 with the GAMMA-LG model of evolution and Bayesian inference phylogenetic trees were obtained using PhyloBayes<sup>83</sup> MPI (version 1.5).

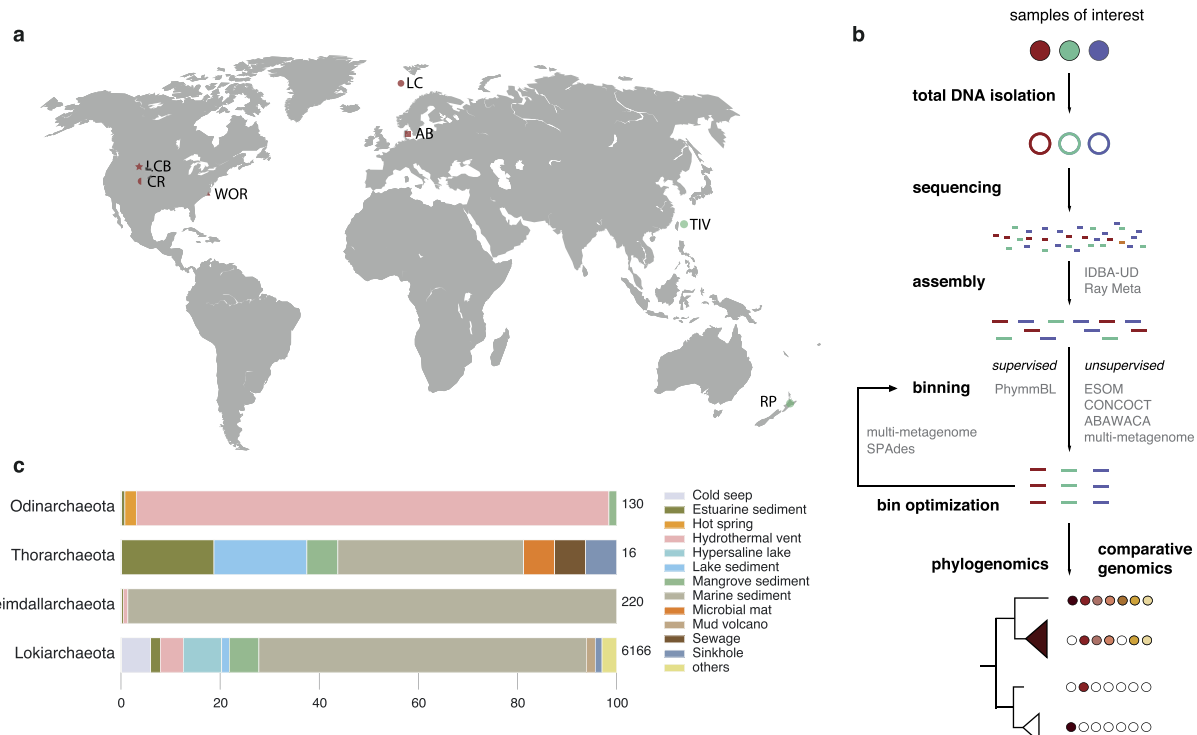
**DNA polymerase B.** Bacterial and eukaryotic sequences were selected based on a previously published dataset<sup>90</sup> and downloaded from NCBI. Archaeal and Asgard polymerase B family proteins assigned to arCOG00328 (PolB3), arCOG00329 (PolB2) and arCOG15272 (PolB1) were added to this dataset after removal of partial and redundant sequences. Sequences were aligned with Mafft-LINSi<sup>80</sup> version 7 and ends were trimmed manually before final trimming using BMGE<sup>81</sup> with the BLOSUM30 matrix. The final alignment (631 positions) was subjected to maximum likelihood phylogenetic inferences using RAxML<sup>77</sup> v.8.0.22 with the GAMMA-LG model of evolution, generating ten independent trees for optimization and 100 slow and non-parametric bootstrap replicates.

**Ribosomal protein L28e.** A representative set of eukaryotic L28e (PF01778) and MAK16 homologues (PF01778 and PF04874) was downloaded from UniProt (Extended Data Fig. 6d). So far, these protein domains have exclusively been found in eukaryotes, with the sole exception of a homologue in *Pontibacillus halophilus*, which was 100% identical to the ribosomal protein L28 of *Chlamydomonas reinhardtii*, indicating contamination. Heimdallarchaeota LC\_3 was the only Asgard representative that encoded a protein with a ribosomal L28e/Mak16 domain (PF01778) but lacking the second N-terminal PF domain characteristic of eukaryotic MAK16 homologues (PF04874). A protein blast against the NCBI database (September 2015) revealed one homologous metagenomic sequence, that was also included in our analysis. All sequences were aligned using Mafft-LINSi<sup>80</sup> version 7, ends were trimmed manually and final trimming was performed trimAl<sup>82</sup> with the gappyout option. The final alignment comprised 122 amino acid positions spanning the first protein domain shared between r-protein L28 and MAK16. Maximum likelihood phylogenetic analyses were performed using RAxML<sup>77</sup> v.8.0.22 with the GAMMA-LG model, generating ten independent trees for optimization and 100 slow and non-parametric bootstrap replicates.

**Data availability.** The genome bins described in this study have been deposited at DDBJ/EMBL/GenBank under the BioProject ID PRJNA319486 and WGS accessions MDVT00000000 (archaeon Odin LCB\_4), MEHG00000000 (Candidatus Thorarchaeota archaeon AB\_25), MEHH00000000 (archaeon Heimdall AB\_125), MDVS00000000 (archaeon Heimdall LC\_3) and MDVR00000000 (archaeon Heimdall LC\_2). The versions described in this paper are versions MDVT01000000, MEHG01000000, MEHH01000000, MDVS01000000 and MDVR01000000, respectively. The Lokiarchaeote CR\_4 bin has been deposited under the BioProject ID PRJNA288027 with WGS accession MBAA00000000 and the version described in this paper is MBAA01000000. The Thorarchaeote bins SMTZ1-83 and SMTZ1-45 are available under BioProject ID PRJNA270657 and WGS accession numbers LRSK00000000 and LRSI00000000.

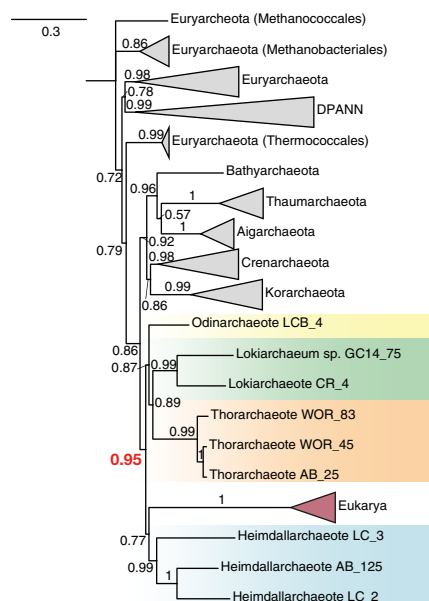
51. Saw, J. H. et al. Exploring microbial dark matter to resolve the deep archaeal ancestry of eukaryotes. *Phil. Trans. R. Soc. Lond. B* **370**, 20140328 (2015).
52. Baker, B. J. et al. Genomic inference of the metabolism of cosmopolitan subsurface Archaea, Hadesarchaea. *Nat. Microbiol.* **1**, 16002 (2016).
53. Castelle, C. J. et al. Genomic expansion of domain Archaea highlights roles for organisms from new phyla in anaerobic carbon cycling. *Curr. Biol.* **25**, 690–701 (2015).

54. Hirayama, H. et al. Culture-dependent and -independent characterization of microbial communities associated with a shallow submarine hydrothermal system occurring within a coral reef off Taketomi Island, Japan. *Appl. Environ. Microbiol.* **73**, 7642–7656 (2007).
55. Lever, M. A. et al. A modular method for the extraction of DNA and RNA, and the separation of DNA pools from diverse environmental sample types. *Front. Microbiol.* **6**, 476 (2015).
56. Bolger, A. M., Lohse, M. & Usadel, B. Trimmomatic: a flexible trimmer for Illumina sequence data. *Bioinformatics* **30**, 2114–2120 (2014).
57. Peng, Y., Leung, H. C., Yiu, S. M. & Chin, F. Y. IDBA-UD: a *de novo* assembler for single-cell and metagenomic sequencing data with highly uneven depth. *Bioinformatics* **28**, 1420–1428 (2012).
58. Boisvert, S., Raymond, F., Godzariadis, E., Laviolette, F. & Corbeil, J. Ray Meta: scalable *de novo* metagenome assembly and profiling. *Genome Biol.* **13**, R122 (2012).
59. Dick, G. J. et al. Community-wide analysis of microbial genome sequence signatures. *Genome Biol.* **10**, R85 (2009).
60. Alneberg, J. et al. Binning metagenomic contigs by coverage and composition. *Nat. Methods* **11**, 1144–1146 (2014).
61. Brady, A. & Salzberg, S. L. Phymm and PhymmBL: metagenomic phylogenetic classification with interpolated Markov models. *Nat. Methods* **6**, 673–676 (2009).
62. Brown, C. T. et al. Unusual biology across a group comprising more than 15% of domain Bacteria. *Nature* **523**, 208–211 (2015).
63. Albertsen, M. et al. Genome sequences of rare, uncultured bacteria obtained by differential coverage binning of multiple metagenomes. *Nat. Biotechnol.* **31**, 533–538 (2013).
64. Bankevich, A. et al. SPAdes: a new genome assembly algorithm and its applications to single-cell sequencing. *J. Comput. Biol.* **19**, 455–477 (2012).
65. Parks, D. H., Imelfort, M., Skennerton, C. T., Hugenholtz, P. & Tyson, G. W. CheckM: assessing the quality of microbial genomes recovered from isolates, single cells, and metagenomes. *Genome Res.* **25**, 1043–1055 (2015).
66. Hyatt, D. et al. Prodigal: prokaryotic gene recognition and translation initiation site identification. *BMC Bioinformatics* **11**, 119 (2010).
67. Markowitz, V. M. et al. IMG: the integrated microbial genomes database and comparative analysis system. *Nucleic Acids Res.* **40**, D115–D122 (2012).
68. Lowe, T. M. & Eddy, S. R. tRNAscan-SE: a program for improved detection of transfer RNA genes in genomic sequence. *Nucleic Acids Res.* **25**, 955–964 (1997).
69. Jones, P. et al. InterProScan 5: genome-scale protein function classification. *Bioinformatics* **30**, 1236–1240 (2014).
70. Marchler-Bauer, A. et al. CDD: NCBI's conserved domain database. *Nucleic Acids Res.* **43**, D222–D226 (2015).
71. Makarova, K. S., Wolf, Y. I. & Koonin, E. V. Archaeal clusters of orthologous genes (arCOGs): an update and application for analysis of shared features between Thermococcales, Methanococcales, and Methanobacteriales. *Life* **5**, 818–840 (2015).
72. Finn, R. D. et al. The Pfam protein families database: towards a more sustainable future. *Nucleic Acids Res.* **44** (D1), D279–D285 (2016).
73. Letunic, I., Doerks, T. & Bork, P. SMART: recent updates, new developments and status in 2015. *Nucleic Acids Res.* **43**, D257–D260 (2015).
74. Söding, J., Biegert, A. & Lupas, A. N. The HHpred interactive server for protein homology detection and structure prediction. *Nucleic Acids Res.* **33**, W244–W228 (2005).
75. Kelley, L. A., Mezulis, S., Yates, C. M., Wass, M. N. & Sternberg, M. J. The Phyre2 web portal for protein modeling, prediction and analysis. *Nat. Protocols* **10**, 845–858 (2015).
76. Pettersen, E. F. et al. UCSF Chimera—a visualization system for exploratory research and analysis. *J. Comput. Chem.* **25**, 1605–1612 (2004).
77. Stamatakis, A. RAxML version 8: a tool for phylogenetic analysis and post-analysis of large phylogenies. *Bioinformatics* **30**, 1312–1313 (2014).
78. Guy, L., Saw, J. H. & Ettema, T. J. The archaeal legacy of eukaryotes: a phylogenomic perspective. *Cold Spring Harb. Perspect. Biol.* **6**, a016022 (2014).
79. Yutin, N., Puigbò, P., Koonin, E. V. & Wolf, Y. I. Phylogenomics of prokaryotic ribosomal proteins. *PLoS One* **7**, e36972 (2012).
80. Katoh, K. & Standley, D. M. MAFFT multiple sequence alignment software version 7: improvements in performance and usability. *Mol. Biol. Evol.* **30**, 772–780 (2013).
81. Criscuolo, A. & Gribaldo, S. BMGE (block mapping and gathering with entropy): a new software for selection of phylogenetic informative regions from multiple sequence alignments. *BMC Evol. Biol.* **10**, 210 (2010).
82. Capella-Gutiérrez, S., Silla-Martínez, J. M. & Gabaldón, T. trimAI: a tool for automated alignment trimming in large-scale phylogenetic analyses. *Bioinformatics* **25**, 1972–1973 (2009).
83. Lartillot, N., Rodrigue, N., Stubbs, D. & Richer, J. PhyloBayes MPI: phylogenetic reconstruction with infinite mixtures of profiles in a parallel environment. *Syst. Biol.* **62**, 611–615 (2013).
84. Nguyen, L. T., Schmidt, H. A., von Haeseler, A. & Minh, B. Q. IQ-TREE: a fast and effective stochastic algorithm for estimating maximum-likelihood phylogenies. *Mol. Biol. Evol.* **32**, 268–274 (2015).
85. Minh, B. Q., Nguyen, M. A. & von Haeseler, A. Ultrafast approximation for phylogenetic bootstrap. *Mol. Biol. Evol.* **30**, 1188–1195 (2013).
86. Guindon, S. et al. New algorithms and methods to estimate maximum-likelihood phylogenies: assessing the performance of PhyML 3.0. *Syst. Biol.* **59**, 307–321 (2010).
87. Viklund, J., Ettema, T. J. & Andersson, S. G. Independent genome reduction and phylogenetic reclassification of the oceanic SAR11 clade. *Mol. Biol. Evol.* **29**, 599–615 (2012).
88. Susko, E. & Roger, A. J. On reduced amino acid alphabets for phylogenetic inference. *Mol. Biol. Evol.* **24**, 2139–2150 (2007).
89. Sukumaran, J. & Holder, M. T. DendroPy: a Python library for phylogenetic computing. *Bioinformatics* **26**, 1569–1571 (2010).
90. Makarova, K. S., Krupovic, M. & Koonin, E. V. Evolution of replicative DNA polymerases in Archaea and their contributions to the eukaryotic replication machinery. *Front. Microbiol.* **5**, 354 (2014).

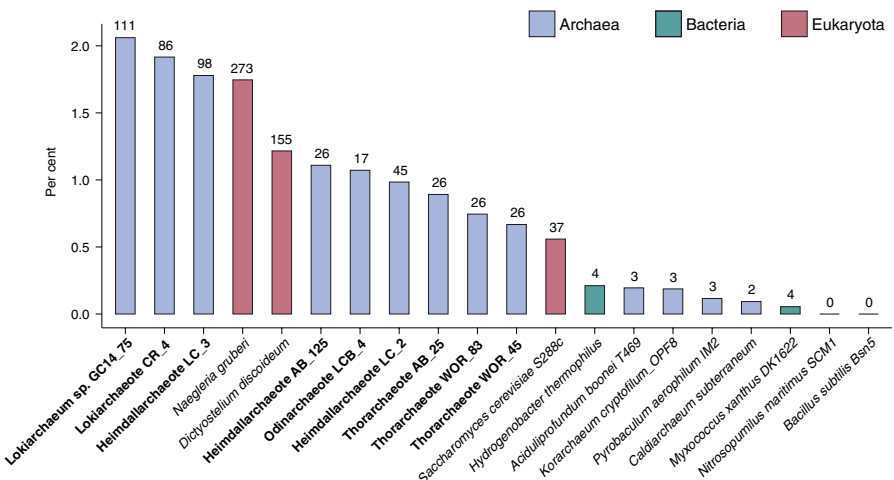


**Extended Data Figure 1 | Sample origin, metagenomics workflow and global distribution of Asgard archaea.** **a**, World map showing the sampling locations of the current study. Abbreviations of the sites mentioned are as follows: LC, Loki's Castle; CR, Colorado River aquifer (USA); LCB, Lower Culex Basin (Yellowstone National Park, USA); WOR, White Oak River (USA); AB, Aarhus Bay (Denmark); RP, Radiata Pool (New Zealand); and TIV, Taketomi Island Vent (Japan). The world

map was drawn using the Matplotlib Basemap Toolkit (<http://matplotlib.org/basemap/>). **b**, Simplified schematic overview of the metagenomics approach that was used to obtain Asgard genomes. Software used during the assembly and binning processes are shown in grey. **c**, Normalized distribution of major Asgard archaeal groups across various environments based on 16S rRNA gene survey datasets. Numbers on the right side of the bar graph represent total number of identified sequences.

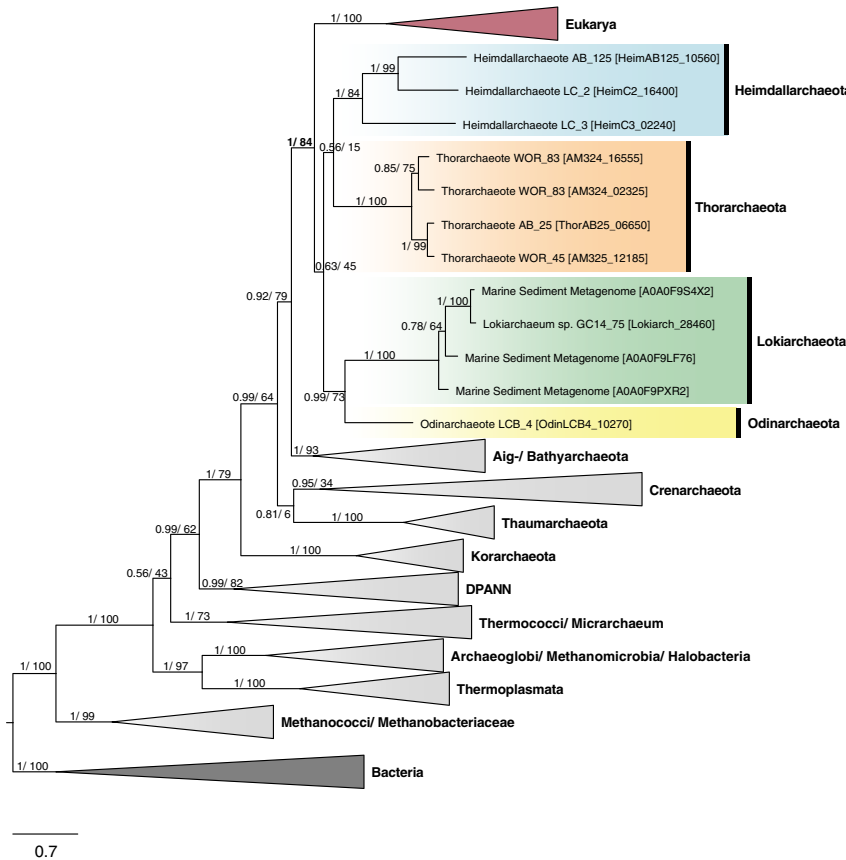


**Extended Data Figure 2 | Bayesian phylogenetic inference of 48 concatenated marker genes.** The tree was inferred using CAT + GTR model and rooted with Bacteria, showing high support for the phylogenetic affiliation between Asgard archaea and eukaryotes (support value in red). Numbers at branches represent posterior probabilities and scale bar indicates the number of substitutions per site.

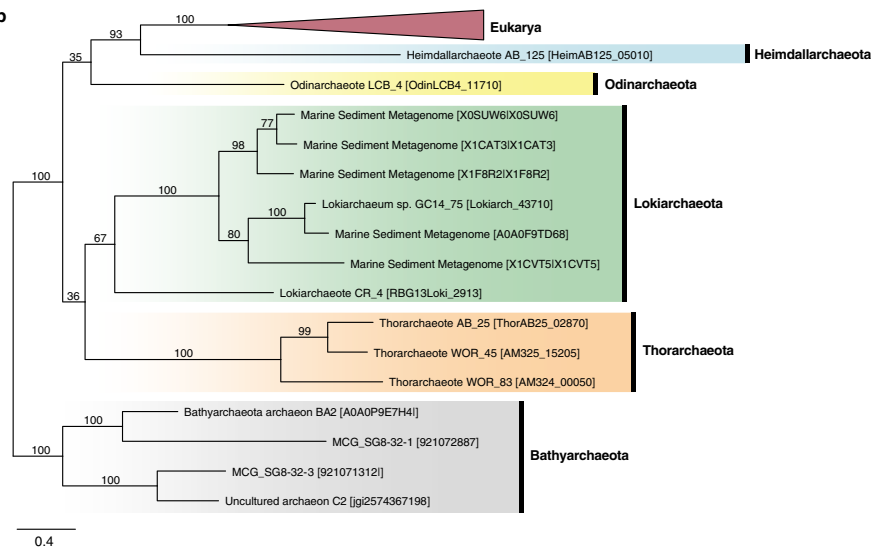


**Extended Data Figure 3 | Asgard genomes encode an expanded GTPase repertoire.** Graph showing small Ras and Arf-type GTPases (containing any of the following domains: IPR006762, IPR024156, IPR006689, IPR006687, IPR001806, IPR003579, IPR020849, IPR003578, IPR021181,

IPR031260, IPR002041, IPR019009) per Asgard genomic bin normalized to the total amount of proteins predicted per genome and compared with selected eukaryotic, archaeal and bacterial taxa. Numbers refer to the total amount of GTPases per genome.

**a**

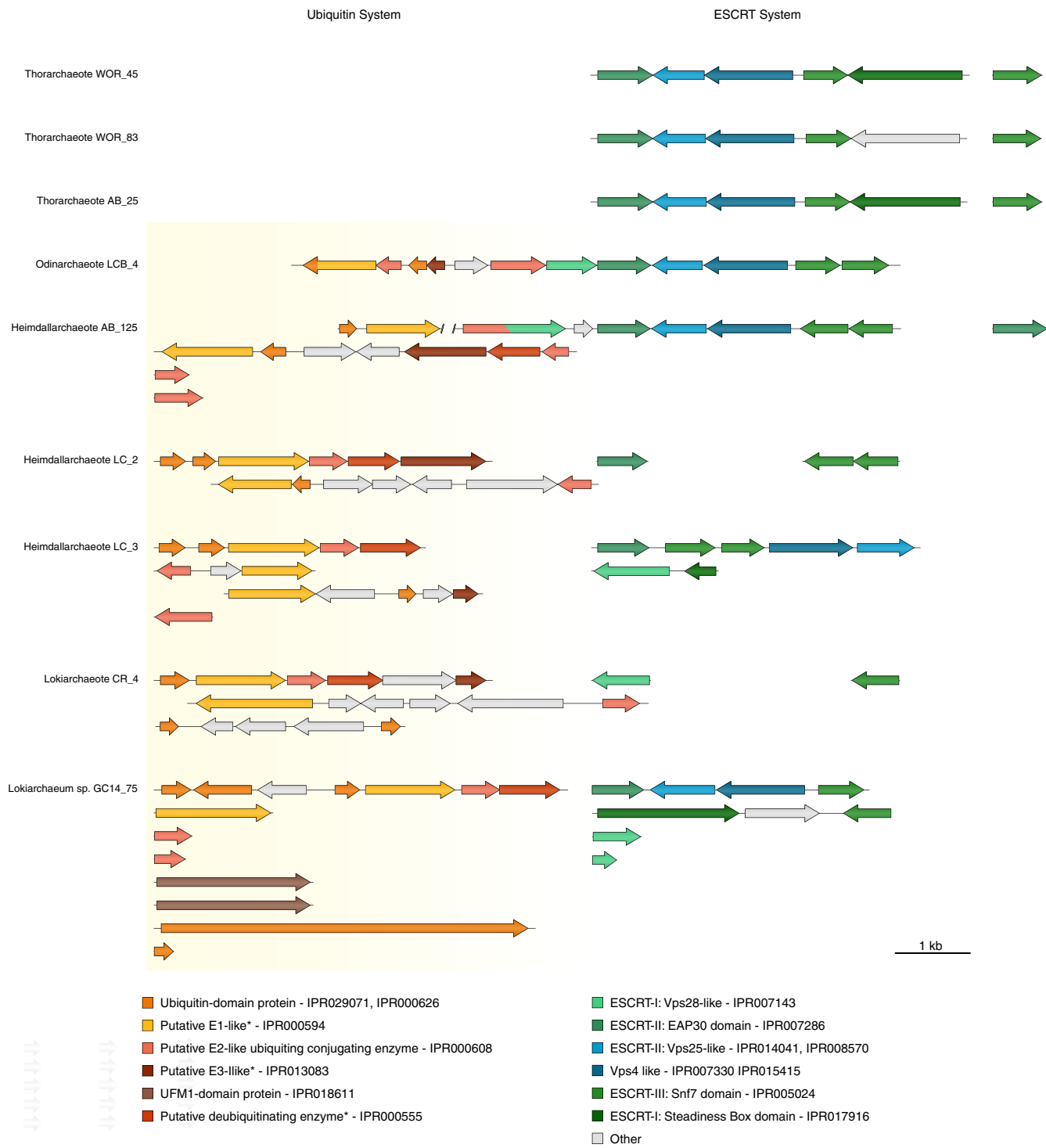
0.7

**b**

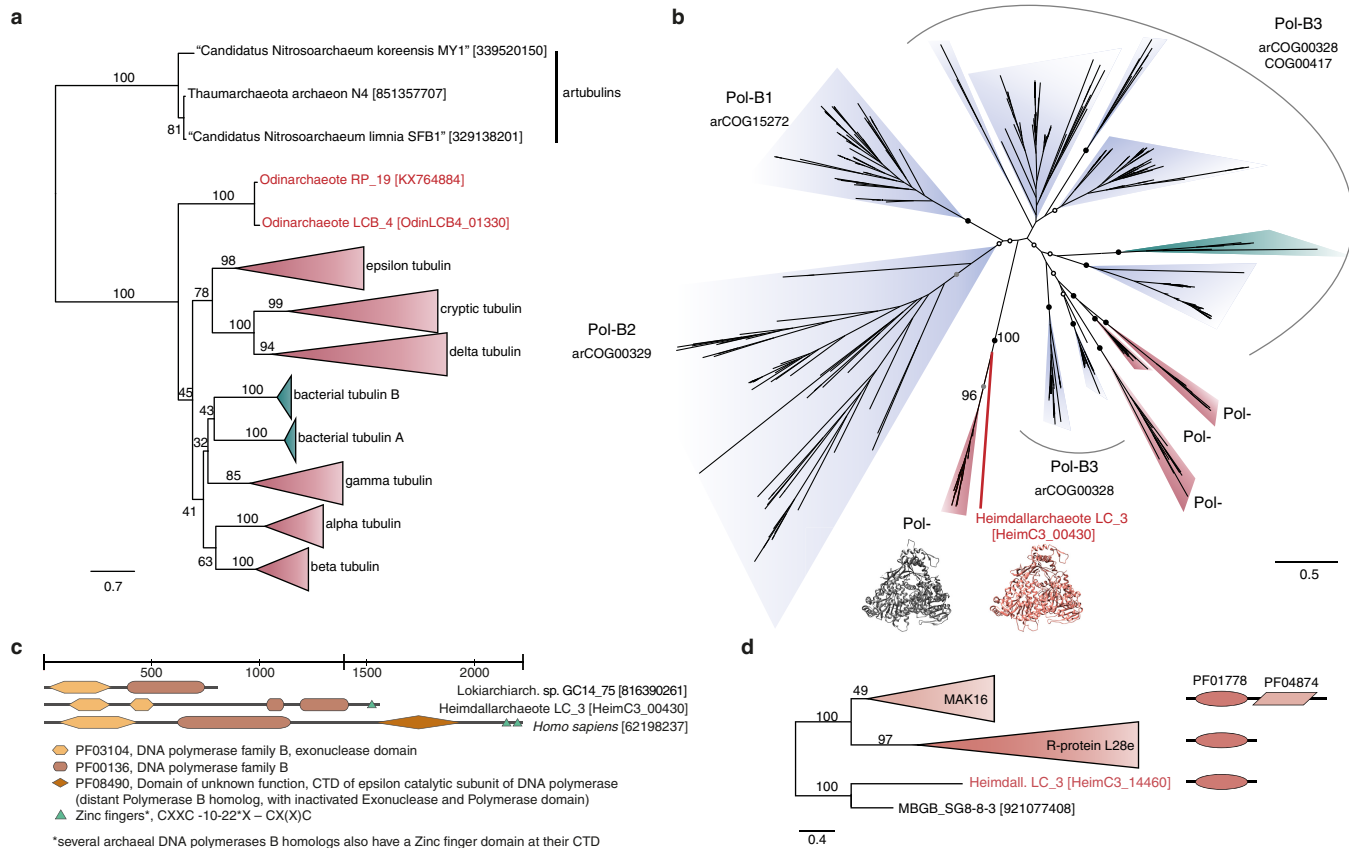
0.4

**Extended Data Figure 4 | Phylogenetic analysis of oligosaccharyl-transferase-complex-related proteins.** **a**, Bayesian inference of STT3-domain proteins (598 aligned amino acid positions) present in all three domains of life. This phylogenetic tree was rooted with bacterial sequences. Numbers at branches refer to Bayesian and non-parametric RAxML bootstrap values, respectively. **b**, Unrooted maximum likelihood

phylogenetic analysis of ribophorin domain proteins (357 aligned amino acid positions) including all prokaryotic homologues identified so far. Numbers at branches show slow, non-parametric maximum-likelihood bootstrap support values. Scale bars indicate the number of substitutions per site.



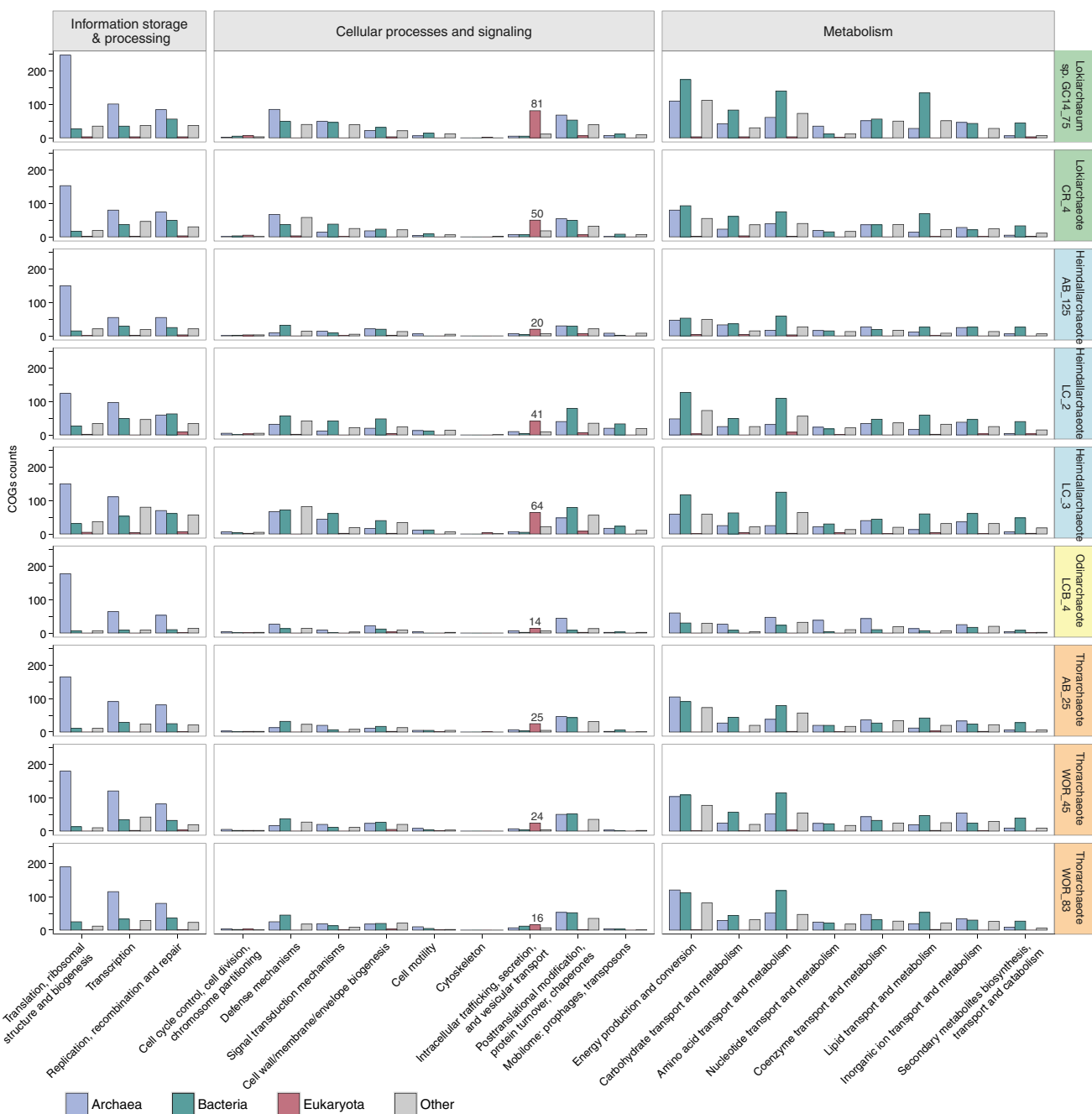
**Extended Data Figure 5 | Genomic conservation links ESCRT and ubiquitin modifier systems.** Schematic overview of ubiquitin and ESCRT gene clusters identified in Asgard genomes. Contiguous contigs from Heimdallarchaeote AB\_125 are represented with a double line at the end of the contig. E1-like and putative deubiquitinating proteins not belonging to any ubiquitin cluster are not shown.



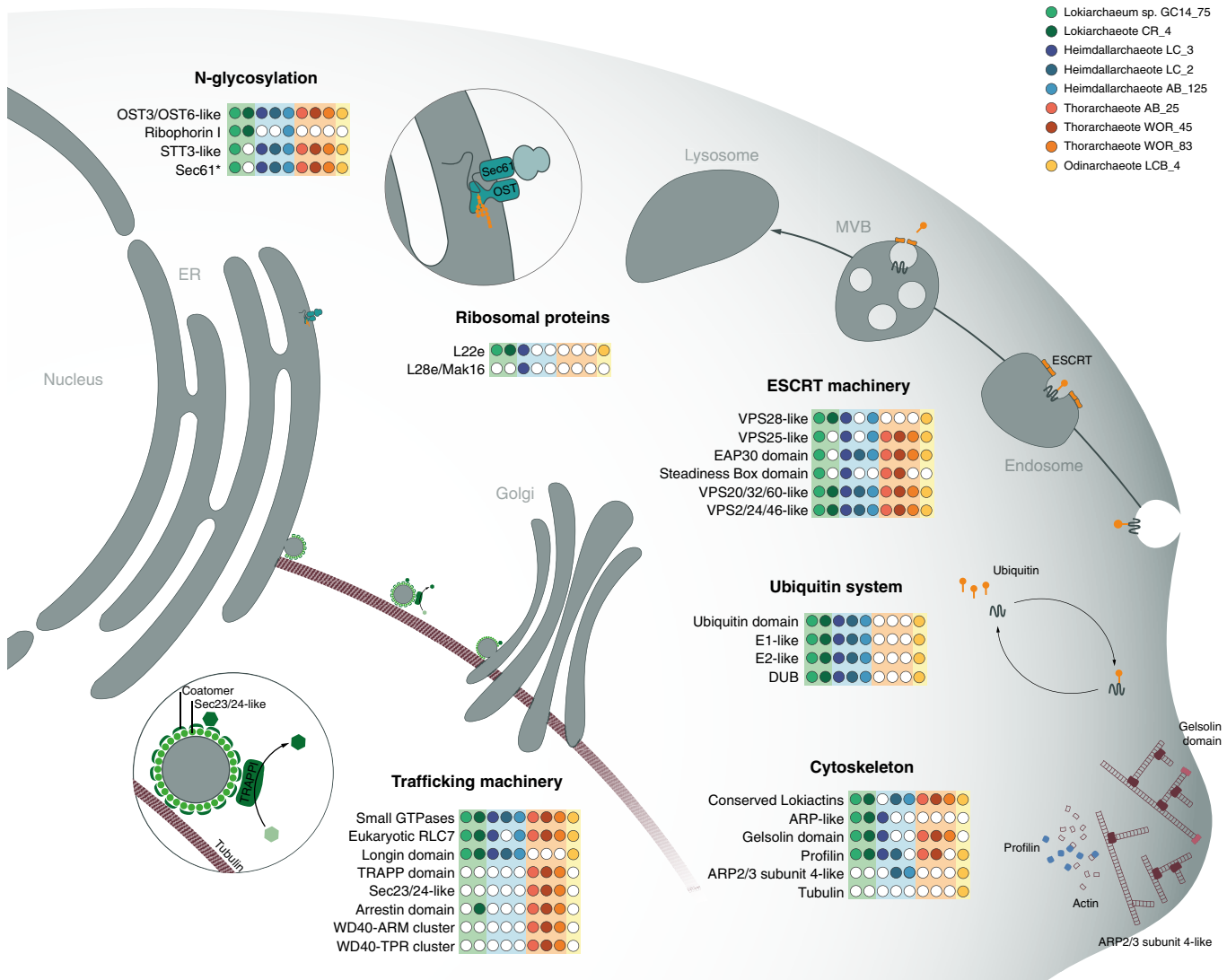
**Extended Data Figure 6 | Phylogenetic analyses of selected ESPs.**

**a**, Tubulin protein family maximum-likelihood tree, highlighting Odinarchaeota homologues branching basal to major eukaryotic tubulin families (red clades). Green clade reflects bacterial tubulin genes probably acquired horizontally from eukaryotes. The tree was rooted with thaumarchaeal artubulins. **b**, Unrooted maximum-likelihood phylogenetic tree of the replicative polymerase B family depicting a Heimdallarchaeote LC\_3 sequence and its corresponding protein model (red), branching basal to the eukaryotic Pol- $\epsilon$  (protein model in grey; PDB ID 4M8O of *S. cerevisiae*). Bootstrap support values of  $\geq 99$ ,  $\geq 90$  and  $\geq 50$  for major clades are indicated by black, grey and white circles, respectively. Eukaryotic, bacterial and archaeal clades are shaded red,

green and purple, respectively. **c**, PFAM domain topology analysis of family B polymerases, indicating that the heimdallarchaeal homologue lacks the C-terminal DUF1744 domain characteristic of eukaryotic Pol- $\epsilon$ . **d**, Unrooted maximum-likelihood tree of RPL28e homologues, including eukaryotic RPL28e and MAK16, a RPL28e-like sequence identified in the Heimdallarchaeote LC\_3 genome and a metagenomic homologue. Eukaryotic MAK16 proteins (implicated in rRNA maturation) contain an additional C-terminal domain absent in the heimdallarchaeal protein. **a, b, d**, Scale bars indicate the number of substitutions per site and numbers at branches show slow, non-parametric maximum-likelihood bootstrap support values.



**Extended Data Figure 7 | Asgard ESPs are enriched for intracellular trafficking and secretion functions.** Overview of functional classification (arCOGs and EggNOG categories) of Asgard proteins assigned to major taxonomic levels. Taxonomic levels are shown in different colours. Note that, in some cases, one protein can be assigned to more than one functional category.



**Extended Data Figure 8 | Eukaryotic signatures in Asgard archaea.** Schematic representation of a eukaryotic cell in which ESPs that have been identified in Asgard archaea are highlighted, including their phylogenetic distribution pattern. The overall picture indicates that the

archaeal ancestor of eukaryotes already contained many key components underlying the emergence of cellular complexity that is characteristic of eukaryotes. DUB, deubiquitinating enzyme; MVB, multi-vesicular body; ER, endoplasmatic reticulum.

Extended Data Table 1 | Assembly statistics and quality metrics of reconstructed Asgard genome bins

	Lokiarchaeota		Thorarchaeota		Odinarchaeota		Heimdallarchaeota		
	CR_4	WOR_83	WOR_45	AB_25	LCB_4	AB_125	LC_2	LC_3	
<b>number of contigs</b>	240	266	119	264	9	225	177	157	
<b>bin size (Mbp)</b>	4.4	3.26	3.54	2.86	1.46	2.28	4.84	5.68	
<b>estimated genome size (Mbp)</b>	5.24	3.08	3.48	3.00	1.52	3.01	6.35	6.23	
<b>N50 (bp)</b>	24155	15333	51214	15359	1181447	10774	38721	59313	
<b>largest contig (bp)</b>	93525	71522	179128	89304	1181447	40319	152089	224298	
<b>GC %</b>	44.22	49.08	42.26	44.55	38.81	33.36	32.75	29.69	
<b>number of ORFs</b>	4488	3407	3513	2915	1584	2348	4586	5514	
<b>completeness (incomplete)</b>	0.78	0.81	0.88	0.83	0.95	0.71	0.68	0.84	
<b>redundancy (incomplete)</b>	1.08	1.30	1.15	1.15	1.01	1.07	1.12	1.09	
<b>completeness (CheckM)</b>	0.81	0.9	0.87	0.9	0.96	0.79	0.72	0.92	
<b>contamination (CheckM)</b>	0.023	0.065	0.051	0.032	0.014	0.023	0.042	0.056	
<b>rRNA</b>	SSU + LSU	SSU + partial LSU	partial SSU + partial LSU	partial SSU + partial LSU	SSU + LSU	SSU + LSU	partial LSU	SSU + partial LSU	

## Extended Data Table 2 | Overview of presence/absence pattern of Asgard ESPs

Description based on arCOG and/or IPRdomain	IPR domain	arCOG	COG	Lokarchaeota CR_4	GC14_75	Thorarchaea WOR_83	WOR_45	Odinar. AB_25	Heimdallarchaeota LCB_4	AB_125	LC_2	LC_3	Comment
<b>Discussed Information processing genes</b>													
Putative DNA polymerase epsilon, catalytic subunit A/POL2	IPR029703*	arCOG00328*	COG00417*	-	-	-	-	-	-	-	-	-	* Heimdallarchaeota LC_3 homolog encodes many additional IPR domains; the one listed here represents the eukaryo-specific IPR domain, which is a signature of Polymerase epsilon; likewise, the arCOGs/COGs also include non-epsilon Polymerases present in other archaea
Eukaryotic-type Topoisomerase IB	several IPR-domains	arCOG08649	COG03569	-	-	◆	◆	◆	-	-	-	-	See phylogeny (Suppl. Fig. 5a). Note: Heimdallarchaeota LC_3 contains a protein, which is distantly related to bacterial Topoisomerase IB and may represent a divergent member of the broader family of DNA breaking-rejoining enzymes (c00213), it is located on a small contig, which may be derived from a pro-viral region
RNA polymerase subunit A, fused	several IPR-domains	arCOG04256;	arCOG04257	COG00086	-	-	-	-	-	-	-	-	◆ See phylogeny (Suppl. Fig. 5b). Although, only the RNA polymerase of Heimdallarchaeota LC_3 is fused, all ASGARDs RNA polymerases form a monophyletic group.
DNA-directed RNA polymerase, subunit RPB8	-	arCOG04271	-	-	-	-	-	-	◆	-	-	-	◆ Based on arCOG assignment, verified using Htpred: Heimdallarchaeota LC_3 homolog retrieves top hit to PF16992: RNA polymerase Rpb8 (E-value: 0.01); value: 6.5E-08, Score: 46.3) and Odinararchaeota LCB_4 homolog shows top hit to pfam03870: RNA polymerase Rpb8 (E-value: 1.4E-49, P-value: 9.3E-55, Score: 297.5)
Putative homologs of eukaryotic ribosomal protein L22e	IPR002671	arCOG22196;	arCOG23043	-	◆	◆	-	-	◆	-	-	-	◆ iPScan did not predict presence of IPR002671/IF001776 in Lokarchaeote CR_4, however we identified a putative homolog in its genome which retrieves a top hit to PF01776 (E-value: 0.044)
Ribosomal L26e/Mak16 family protein	IPR029004	-	-	-	-	-	-	-	-	-	-	-	◆ See phylogeny (Ext. Data Fig. 6d). Putative homolog of eukaryotic ribosomal protein L26e/MAK16 (SMART retrieves top hit to PF01776 E-value: 2.7e-09)
<b>Cell division/ cytoskeleton related proteins</b>													
Conserved actin-like	IPR004000; IPR020902*	various arCOGs	various COGs	◆	◆	◆	◆	◆	◆	◆	◆	◆	See phylogeny (Suppl. Fig. 2a and b). One of the actin homologs of all ASGARDs is highly conserved, while the other homologs seem to represent more divergent ARPs; *IPR020902 is only detected in the conserved actin of Lokarchaeote CR_4, Lokarchaeum sp. GC14_75, Odinararchaeota LCB_4 and all Thorarchaeota
Several additional bona fide actin-like proteins	IPR004000	-	-	◆	◆	-	-	-	-	-	-	-	◆
Gelsolin family domain proteins	IPR07122; IPR007123; IPR029006; IPR29919*; IPR030004*	arCOG20384	-	◆	◆	◆	◆	◆	-	-	-	-	*IPR29919 detected in Heimdallarchaeota LC_3 and thorarchaeal homologs; *IPR030004 only detected in a gelsolin homolog of Lokarchaeote CR_4
Profilin domain proteins	IPR005455	arCOG20397/ arCOG22203	-	◆	◆	◆	◆	◆	◆	◆	◆	◆	Thorarchaeote WOR_83 encodes homologous proteins that have been assigned to the same arCOG; however, iPScan did not predict the presence of IPR005455
Tubulin, Beta Tubulin and	IPR000217; IPR002453; IPR02123*	arCOG02202	COG00206	-	-	-	-	-	◆	-	-	-	See phylogeny (Ext. Data Fig. 6a). Odinararchaeota LCB_4 homolog has several additional IPR domains, here only the tubulin specific IPR domains are given; the arCOG/COG families correspond to the larger FtsZ (cell division GTPase) family widely distributed in bacteria and several archael phyla including ASGARDs with Odinararchaeota LCB_4.
Actin-related protein 2/3 complex subunit 4	IPR008384	-	-	-	-	-	-	-	◆	◆	-	-	Heimdallarchaeota LC_2 and Odinararchaeota LCB_4 might contain homologs of this protein as identified by blast; however, the IPR domain was not predicted by iPScan; in contrast the smart database recovers hits to potential Arp2/3 complex subunits, though with high E-values: 0.9 (Heimdallarchaeota LC_2) and 3e-4 (Odinararchaeota LC_2)
<b>ESCRT machinery</b>													
Vps4 ATPase with characteristic M-domain	IPR007330 and IPR015415	arCOG01307	COG00464	(-)	◆	◆	◆	◆	◆	◆	◆	◆	No ESP. Some proteins containing the M1 domain (IPR007330) but lacking IPR015415 can also be found in Lokarchaeote CR_4, Thorarchaeote WOR_45 and Lokarchaeum sp. GC14_75
Vps20/3280-like protein (ESCRT-III)	IPR005024	various arCOGs	-	◆	◆	◆	◆	◆	◆	◆	◆	◆	See phylogeny (Suppl. Fig. 3a and b)
Vps24/246-like protein (ESCRT-III)	IPR005024	various arCOGs	-	◆	◆	◆	◆	◆	◆	◆	◆	◆	◆
EAP30 domain protein (ESCRT-II) (Vps22/26-like)	IPR007286	arCOG20068 and/or arCOG21604	-	(-)	◆	◆	◆	◆	◆	◆	◆	◆	Putative EAP30 domain seems to be present in Lokarchaeote CR_4 (found by blastp), however, this candidate protein does not retrieve significant hits in protein databases and its length highly differs from the rest of the proteins found.
Vps25-like protein (ESCRT-I)	IPR014041; IPR008570	arCOG20069	-	◆	◆	◆	◆	◆	◆	◆	◆	◆	◆
Hypothetical protein with Vps28-like domain	IPR007143	-	◆	◆	-	-	-	-	◆	◆	◆	◆	◆
Protein with putative steadfastness box domain	IPR017916	arCOG20388	-	(-)	◆	(-)	◆	◆	-	-	-	-	See Blast or gene cluster (Ext. Data Fig. 5) Steadfastness box part of Vps23 in Eukaryotes; homologs of this protein that do not give hits to the steadfast box present in Lokarchaeote CR_4 and Thorarchaeote WOR_83 (arCOG20388) and part of the ESCRT gene clusters; the homolog of Heimdallarchaeota LC_3 is partial
Cyclin-like; Cyclin, N-terminal	IPR013763; IPR006671	-	-	-	-	-	-	-	-	-	-	-	The cyclin-like domain is found in eukaryotes, but it is also found as the core domain in transcription factor IIB (TFIIB) (Nikolic et al., 1995, Nature). This domain is also detected in 2 sequences of archaeal TFIIB. The Heimdallarchaeota LC_3 homolog does however not retrieve significant blast hits and is located next to the ESCRT cluster
Putative BRO1 domain protein	IPR004328	arCOG21565	-	-	-	-	-	-	◆	◆	-	-	Involves in protein targeting to the vacuole or lysosome in some eukaryotes; interacts with ESCRT-III; the IPR domain is however predicted only in Heimdallarchaeota AB_125
<b>Ubiquitin modifier system</b>													
Ubiquitin-related domain; Ubiquitin-like RWD domain	IPR029071; IPR000626	various arCOGs	-	◆	◆	-	-	-	◆	◆	◆	◆	See phylogeny (Suppl. Fig. 4). The IPR000594 domain represents a NAD/FAD-binding fold found in the ubiquitin activating E1 family but also in members of the bacterial Thf/Moef/BhesA family, not ESP; here indicated are only those NAD/FAD-binding fold proteins that occur in ubiquitin gene cluster and cluster phylogenetically with the eukaryotic E1 ligase family.
Candidates for Ubiquitin-activating enzymes E1	IPR000594 if encoded in ubiquitin gene cluster	arCOG01676	COG00476	◆	◆	-	-	-	◆	◆	◆	◆	◆
Ubiquitin-activating enzyme (E1), catalytic cysteine domain	IPR019572 (IPR000594)	arCOG01676	COG00476	◆	◆	-	-	-	-	-	-	-	◆
E2 binding domain	IPR014929 (IPR02318) (IPR000594)	arCOG01676	COG00476	-	-	-	-	-	-	-	-	-	This domain is present in eukaryotic NEDD8 activating E1 enzymes
Putative E2-like ubiquitin conjugating protein	IPR000608	various arCOGs	-	◆	◆	-	-	-	◆	◆	◆	◆	In one protein of Heimdallarchaeota AB_125, this domain is fused to VPS28 domain (IPR007143)
E3 UFM1-protein ligase 1 domain	IPR018611	-	-	-	◆	-	-	-	-	-	-	-	Canonical E3-like ligase domain
Zinc finger, RING/FYVE/PHD-type	IPR013083	various arCOGs	-	◆	◆	◆	◆	◆	◆	◆	◆	◆	No ESP. Candidates for E3 ligases.
JAB1/MPN/MOV34 metalloenzyme domain	IPR000555 without IPR028090	various arCOGs	-	◆	◆	-	-	-	◆	◆	◆	◆	No ESP. IPR000555 together with IPR028090 domain are also present in Thorarchaea and other Asgards (JAB domain, prokaryotic). Here we just show the presence of the IPR000555 domain proteins that do not have the IPR028090 domain and that show closest relationship to eukaryotic homologs (by blastp)
<b>Trafficking system-related proteins</b>													
Plethora of Ras-superfamily GTPases	diverse domains	arCOG00362	COG02229	◆	◆	◆	◆	◆	◆	◆	◆	◆	See figure for abundance overview and detailed list of small GTPases (Ext. Data Fig. 3, Suppl. Table 8). Most small GTPases of the ASGARDs have been assigned to this very broad arCOG/COG class
Rag-type GTPase domain signature	IPR006762*	arCOG00362	COG02229	◆	◆	-	-	-	◆	◆	◆	◆	* All small GTPases contain several IPR domains, here only a specific characteristic domain is listed
Signal recognition particle receptor, beta subunit domain	IPR019009	-	-	-	-	-	-	-	-	-	-	-	A Rag-type GTPase?
Eukaryotic-like RLC7 roadblock domain protein	IPR004942 and/or IPR015019	diverse arCOGs	COG02018 or none	◆	◆	◆	◆	◆	◆	◆	◆	◆	See phylogeny (Suppl. Fig. 1a and b). Like other archaea and bacteria, ASGARD archaea encode diverse roadblock domain proteins. Indicated here are thus only those roadblock domain proteins that are more similar to the eukaryotic RLC7 family than to the bacterial/archaeal roadblocks and are characterized by the lack of the last alpha helix (Klinger et al., 2016).
Longin-like domain and/or MON1 domain proteins	IPR011012, IPR004353	diverse arCOGs	-	◆	◆	(-)	(-)	(-)	◆	◆	◆	◆	Heimdallarchaeota LC_3 contains only one candidate protein with MON1 domain fused to a low complexity transmembrane protein; homologs of longin-like domain and/or MON1 domain to IPR011012 are not detected. Interestingly, the Heimdallarchaeota LC_3 homolog of Thorarchaeota longin suggests that these are more divergent such that the IPR domain is not picked up by iPScan, neither (see Klinger et al., 2016).
Transport protein particle (TRAPP) component	IPR007194 (IPR024096)	arCOG00861 or arCOG01688 (COG01719)	-	-	◆	◆	◆	◆	-	-	-	-	See phylogeny (Fig. 2a and b) Thorarchaeote WOR_45 and AB_25 encode two protein homologs with a eukaryotic transport protein particle (TRAPP) component domain, which is present in eukaryotic Transport protein particle complex subunits 3, 5 and 6. These thorarchaeal homologs occur in a gene cluster together with a more distantly related V4R domain protein (IPR024096), homologs of which are also found in other archaea and bacteria. (Podar et al., 2006)
Zinc finger, Sec23/Sec24-type; Sec23/Sec24 trunk domain; Sec23/Sec24 beta-sandwich	IPR006895; IPR006996; IPR02990	arCOG02900*	COG02304*	-	◆	◆	◆	◆	-	-	-	-	See phylogeny and protein domain architecture (Fig. 2c and d). ArCOG/COG comprises von Willebrand factor domain proteins, which are also encoded by other archaea, however, these do not encode the Sec23/24 signature IPR domains.
WD40 repeat domain located next to WD40 repeat domain (alpha solenoid); (Potential candidates for Sec13/31 candidate/cotamer alpha/beta subunit candidates ?)	Armadillo repeat; IPR01989; IPR016024; WD40 repeat; IPR020022; IPR01788; IPR01945; IPR01980; IPR019775	Armadillo repeat; arCOG02316 (?) WD40 arCOG02319	-	◆	◆	◆	◆	◆	-	-	-	-	See gene clusters and results for phage models (Fig. 2f and Suppl. Table 9). E-value for domain hit for Thorarchaeote AB_25: 1.1E-4; however, IPR01989 and IPR016024 are not detected by iPScan, whereas IPR020022, IPR01788, IPR01945, IPR01980 and IPR019775 encodes a WD40 repeat protein, which also retrieves hits to the epsilon subunit of cotamers. Interestingly, however, in Thorarchaeote WOR_45 and AB_25 this protein is located next to a WD40 domain protein and might represent another candidate for a putative archaeal "protocotamer".
TPR repeat protein with remote similarity to coatomer, epsilon subunit	IPR006822	arCOG00948 or arCOG005137	COG00457	-	◆	-	◆	(-)	◆	-	-	-	C- and N-terminals of arrestin seem to be homologous to each other (fall within same ASGARD specific arCOG, and both have immunoglobulin-like beta-sandwich structure); each of the putative N- or C-terminal arrestin domain proteins of ASGARDs comprises a separate protein. In Lokarchaeote CR_4, the N- and C-terminal arrestin-like domain proteins are located next to each other with one gene separator, however, in Thorarchaeote WOR_45 they are located on different genes. Interestingly, the C-terminal arrestin domain protein is predicted to interact with the N-terminal arrestin domain protein via a G-protein coupled receptor. NOTE: also one member of the Bathyarchaeota is predicted to encode an arrestin-domain protein: AC477_00690
Arrestin-like proteins ("C-terminal" domain-like)	IPR011021 (IPR014756)	arCOG20411	-	◆	-	◆	◆	◆	-	-	-	-	See phylogeny (Ext. Data Fig. 4b). In grey indicated are Olinarchaeota LCB_4 and Thorarchaeota homologs that do not encode the canonical IPR domains, yet are homologous based on phylogenetic analysis.
Arrestin-like proteins ("N-terminal" domain-like)	IPR014752 (IPR014756)	arCOG20411	-	◆	-	-	-	-	-	-	-	-	See phylogeny (Ext. Data Fig. 4a). Thorarchaeote WOR_83: two copies; this domain is also found in genomes of Bathyarchaeota and Thermoprotei
<b>Oligosaccharide-transferase complex</b>													
Ribophorin I	IPR007676	arCOG20142	-	◆	◆	◆	◆	◆	◆	◆	◆	◆	See phylogeny (Ext. Data Fig. 4b). In grey indicated are Olinarchaeota LCB_4 and Thorarchaeota homologs that do not encode the canonical IPR domains, yet are homologous based on phylogenetic analysis.
Oligosaccharide transferase complex, subunit OST3/OST6	IPR021149	arCOG20107	-	◆	◆	◆	◆	◆	◆	◆	◆	◆	See phylogeny (Ext. Data Fig. 4a). Thorarchaeote WOR_83: two copies; this domain is also found in genomes of Bathyarchaeota and Thermoprotei
Oligosaccharide transferase, STT3 subunit	IPR003674	arCOG2044	COG01287	-	◆	◆	◆	◆	◆	◆	◆	◆	See phylogeny (Ext. Data Fig. 4a). Thorarchaeote WOR_83: two copies

Presence of genes is indicated by diamonds. See comments in column 14 for a detailed explanation for each domain/protein family.